Gutzwiller projection for exclusion of holes: Application to strongly correlated ionic Hubbard model and binary alloys

Anwesha Chattopadhyay* and Arti Garg†
Condensed Matter Physics Division, Saha Institute of Nuclear Physics, HBNI, 1/AF Bidhannagar, Kolkata 700 064, India

(Received 5 January 2018; published 11 June 2018)

We consider the strongly correlated limit of variants of the Hubbard model in which on parts of the system it is energetically favorable to project out doublons from the low-energy Hilbert space while on other sites of the system it is favorable to project out holes while still allowing for doublons. As an effect the low-energy Hilbert space itself varies with sites of the system. Though the formalism is well developed for the case of doublon projection in the literature, the case of hole projection has not been explored in detail so far. We derive the basic framework by defining creation and annihilation operators for electrons in a restricted Hilbert space where holes are projected out but which still allows for doublons. We generalize the idea of the Gutzwiller approximation for the case of hole projection, which has been done in the literature for the case of doublon projection. To be specific, we provide a detailed analysis of the strongly correlated limit of the ionic Hubbard model which has a staggered potential Δ on two sublattices of a bipartite lattice and the correlated binary alloys which have binary disorder $\pm V/2$ randomly distributed on sites of the lattice. In both cases, for $\Delta \sim U \gg t$ and for $V \sim U \gg t$, where U is the Hubbard energy cost for having a doublon at a site, there are sites on which doublons are allowed while holes are the maximum energy states. We do a systematic generalization of similarity transformation for both these cases and obtain the effective low-energy Hamiltonian. We further derive Gutzwiller approximation factors which provide renormalization of various terms in the effective low-energy Hamiltonian due to the Gutzwiller projection operators, excluding holes on some sites and doublons on the remaining sites.

DOI: 10.1103/PhysRevB.97.245114

I. INTRODUCTION

Strongly correlated systems are of immense interest and importance in condensed matter physics. Strong e-e interactions leads to many interesting phases like high-T_c superconductivity, antiferromagnetically ordered phases, and Mott insulators. The Hubbard model is a paradigmatic model in strongly correlated electron systems with two simple ingredients, namely, hopping of electrons ($\sim t$) and on-site Coulomb interaction ($\sim U$). In the limit of large U and finite hole doping, doublons are energetically unfavorable and need to be projected out from the low-energy Hilbert space. A regular similarity transformation which projects out double occupancies gives the effective low-energy Hamiltonian which is known as the t-J model [1] and captures many aspects of the physics of high-T_c superconducting cuprates [2].

The t-J model is defined in the projected Hilbert space and since Wick's theorem does not work for the fermionic operators in the projected Hilbert space, standard many-body physics tools of calculating various order Feynman diagrams for the self-energy [3] cannot be used to solve this model. One needs to solve the Schwinger equation of motion for the Green's function of projected electrons [4] and use a systematic perturbation theory in some parameter that controls double occupancy. Numerically, the t-J model can be studied using the variational Monte Carlo method [5] where one starts with a variational wave function and then carries out doublon projection from each site explicitly. But because of the computational complexity, another alternative analytical tool most commonly used in the community as an approximate way of implementing the projection of double occupancies is known as the Gutzwiller approximation. The Gutzwiller approximation, as first introduced by Gutzwiller [6], was improved and investigated later by several others [7] mainly in the context of the hole-doped t-J model. Under this approximation, the expectation value in the projected state is related to that in the unprojected state by a classical statistical weight factor know as the Gutzwiller factor that accounts for doublon exclusion. As an effect various terms in the Hamiltonian become renormalized by the Gutzwiller factors and the renormalized Hamiltonian can be studied in the unprojected basis.

Though the Gutzwiller projection for exclusion of doublons has been explored in detail in the literature, the Gutzwiller projection of holes from the low-energy Hilbert space and its implementation in renormalizing the couplings in the effective low-energy Hamiltonian at the level of the Gutzwiller approximation are still completely unexplored. There are models, like the electron-doped t-J model, where in the low-energy Hilbert space one has to allow for doublons and holes have to be excluded. But in this situation it is not really essential to use the formalism of the Gutzwiller projection for holes as one can simply do particle-hole transformation and map the model to the hole-doped t-J model where the low-energy Hilbert space allows for holes excluding doublons. But there are situations where the Gutzwiller projection of holes becomes crucial to

*anwesha.chattopadhyay@saha.ac.in
†arti.garg@saha.ac.in

carry out, e.g., in a model where on some of the sites it is energetically favorable to do hole projection while on some other sites doublon projection is required. With this motivation, we provide the basic formalism for the Gutzwiller projection of holes and calculate the Gutzwiller factors for implementing this projection approximately by renormalizing the couplings in the low-energy Hamiltonian for a couple of such models.

In this work we provide a general formalism for studying variants of the strongly correlated Hubbard model with inhomogeneous on-site potential terms of the same order as U or larger than that. Due to competing effects of on-site potential and U, there are sites at which holes are the maximum energy states (rather than doublons) and should be projected out from the low-energy Hilbert space. We do a systematic extension of the similarity transformation in which the similarity operator itself varies from bond to bond depending upon whether both sites of the bond have doublon-projected low-energy Hilbert space dominated by large-U physics, or both have hole-projected low-energy Hilbert space, or one of the sites on the bond has a hole-projected and the other site has a doublon-projected low-energy Hilbert space. We further calculate generalized Gutzwiller approximation factors for various terms in the low-energy effective Hamiltonian which are also bond dependent. Gutzwiller factors for bonds where one site requires hole projection and the other has doublon projection or where both the sites have hole projection have not been calculated in the literature earlier and in this work we derive them under the assumption that spin-resolved densities before and after the projection remain the same.

To be specific, we provide details of the formalism for two well-studied models, namely, the ionic Hubbard model (IHM) and correlated binary alloys represented by the Hubbard model in the presence of binary disorder. IHM is an interesting extension of the Hubbard model with a staggered on-site potential Δ added onto it. IHM has been studied in various dimensions with a variety of numerical and analytical tools. In one dimension [8], it has been shown to have a spontaneously dimerized phase, in the intermediate-coupling regime, which separates the weakly coupled band insulator from the strong-coupling Mott insulator. In higher dimensions ($d > 1$), this model has been studied mainly using dynamical mean field theory (DMFT) [9–16], determinantal quantum Monte Carlo [17,18], cluster DMFT [19], and the coherent potential approximation [20]. Though the solution of DMFT self-consistent equations in the paramagnetic (PM) sector at half filling at zero temperature shows an intervening metallic phase [10], in the spin-asymmetric sector, the transition from paramagnetic band insulator (PM BI) to antiferromagnetic (AFM) insulator preempts the formation of a parametallic phase [12,19]. In a recent work coauthored by one of us, it was shown that upon doping the IHM one gets a broad ferrimagnetic half-metal phase [13] sandwiched between a PM BI and a PM metal. IHM has also been realized in optical lattices [21] on the honeycomb structure.

Most of these earlier works on IHM are in the limit of weak to intermediate U/t except [14,16] where the strongly correlated limit of IHM has been studied for $\Delta \leqslant U$ within DMFT. Recently [22] the $\Delta \sim U \gg t$ limit of IHM has been studied using slave-boson mean field theory. The Gutzwiller approximation method has been used for studying IHM [23] but in the limit of large U (not extreme correlation limit) where double occupancies are not fully prohibited. To the best of our knowledge, the Gutzwiller approximation formalism for this model has not been developed in the limit $\Delta \sim U \gg t$ which we present in this work. In the limit of large U and Δ ($U \sim \Delta$), holes are energetically expensive in the sublattice where the staggered potential is $-\Delta/2$ (say, sublattice A) and double occupancies are expensive in the sublattice having potential $\Delta/2$ (say, B). Therefore holes are projected out from the A sublattice and doublons from the B sublattice, which gives us the low-energy effective Hamiltonian.

The second model for which we provide details of the formalism is the model of correlated binary alloys described by the Hubbard model in the presence of the binary disorder potential. In all correlated electron systems, disorder is almost inevitable due to various intrinsic and extrinsic sources of impurities. In high-T_c cuprates, it is the doping of the parent compound (e.g., with oxygen) which results in the random on-site potential along with introducing holes [24]. Another type of common disorder is binary disorder which is for example realized in disulfides ($Co_{1-x}Fe_xS_2$ and $Ni_{1-x}Co_xS_2$) [25] in which two different transition metal ions are located at random positions, creating two different atomic levels for the correlated d electrons. Binary disorder along with interactions among basic degrees of freedom has also been realized in optical lattice experiments [26]. Hence it becomes crucial to study the interplay of disorder and interactions in order to understand many interesting properties of these systems.

In the correlated binary alloy model, the on-site potential can be $\pm V/2$ at any site of the lattice randomly. The physics of this model has been explored for the intermediate to strong coupling regime mainly using DMFT [27–30]. But the limit of large on-site repulsion as well as strong disorder potential $U \sim V \gg t$, where holes are projected out from sites having potential $-V/2$ (A) sites and double occupancies are projected out from sites having potential $V/2$ (B) sites, has not been explored so far. Though this model has similarity with the IHM mentioned above, the intrinsic randomness associated with the binary disorder model makes the effective low-energy Hamiltonian different from the case of IHM. The interplay of disorder and interaction in this model may lead to very different physics like many-body localization [31].

The rest of the paper is structured as follows. First we provide the basic formalism for hole projection by defining electron creation and annihilation operators in the hole-projected Hilbert space. We enlist probabilities of various allowed configurations in the hole-projected Hilbert space and calculate the Gutzwiller approximation factors for hopping processes. In the next section, we have derived the effective low-energy Hamiltonian for the IHM in the limit of $U \sim \Delta \gg t$ and calculated the corresponding Gutzwiller approximation factors for various terms in the Hamiltonian. Followed by this we have described the similarity transformation and Gutzwiller approximation for correlated binary alloys in the limit of strong interactions and strong disorder. At the end, we also touch upon the case of fully random disorder and randomly distributed attractive impurities in the limit of both interaction and disorder strength being much larger than the hopping amplitude.

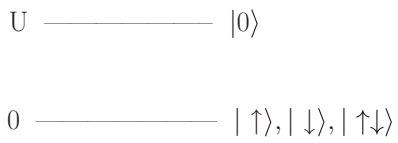

FIG. 1. Separation in the energy scales of a hole and other states.

II. BASIC FORMALISM FOR HOLE PROJECTION

Though the formalism of Gutzwiller projection is well developed for the case of doublon projection in the literature, case of hole projection has not been explored in detail so far. In this section we derive the basic framework by defining new creation and annihilation operators for electrons in a restricted Hilbert space where holes are projected out but which still allows for doublons.

For a system of spin-1/2 fermions, at each site there are four possibilities, namely, $|\uparrow\rangle$,$|\downarrow\rangle$,$|\uparrow\downarrow\rangle$, and $|0\rangle$. Consider a model in which the energy cost of having $|0\rangle$ is much more than the other three states, e.g., shown in Fig. 1. It may also happen that due to some other constraints, e.g., to achieve certain density of particles in the system, one has to retain doublons in the low-energy Hilbert space (though the energy cost for doublons might be close to that of holes) and exclude holes. In these situations, the effective creation and annihilation operators for fermions in the low-energy Hilbert space need to be modified.

The simplest way to see this is the following. A normal electron creation operator can be expressed in terms of local Hubbard operators:

$$c_\sigma^\dagger = X^{\sigma\leftarrow 0} + \eta(\sigma) X^{d\leftarrow\bar{\sigma}}, \tag{1}$$

where σ can be $\uparrow$ or $\downarrow$ and d represents a double occupancy and $\eta(\uparrow) = 1$ and $\eta(\downarrow) = -1$. Here we have used the local Hubbard operators defined as $X^{b\leftarrow a} = |b\rangle\langle a|$.

This means one can create a particle either starting from a hole or by annihilating one particle from a double occupancy. Since in the present case holes are projected out from the low-energy subspace, one cannot create a particle starting from a hole; rather we can create a particle only by annihilating one particle from a doublon. Therefore, the projected electron creation operator, which we denote by $\tilde{c}_\sigma^\dagger$, is

$$\tilde{c}_\sigma^\dagger = \eta(\sigma) X^{d\leftarrow\bar{\sigma}} = c_\sigma^\dagger n_{\bar{\sigma}} \tag{2}$$

with $\eta(\uparrow) = 1$ and $\eta(\downarrow) = -1$. Note that $\tilde{c}_\sigma$ does not satisfy standard Lie algebra of fermions but $\{\tilde{c}_\sigma,\tilde{c}_\sigma^\dagger\} = n_{\bar{\sigma}}$. The corresponding number operator in this reduced Hilbert space is $\tilde{n}_\sigma = n_\sigma n_{\bar{\sigma}}$. Various Hubbard operators in terms of a fermionic operator in hole-projected Hilbert space are given as $X^{\sigma\leftarrow\sigma} = \tilde{c}_{\bar{\sigma}}\tilde{c}_{\bar{\sigma}}^\dagger$, $X^{\sigma\leftarrow\bar{\sigma}} = -\tilde{c}_{\bar{\sigma}}\tilde{c}_\sigma{}^\dagger$, and $X^{d\leftarrow d} = \tilde{c}_\uparrow^\dagger\tilde{c}_\uparrow = \tilde{c}_\downarrow^\dagger\tilde{c}_\downarrow$. From the completeness relation of X operators in hole-projected Hilbert space we get

$$\begin{aligned} X^{\uparrow\leftarrow\uparrow} + X^{\downarrow\leftarrow\downarrow} + X^{d\leftarrow d} &= \mathcal{I}, \\ n_\uparrow(1-n_\downarrow) + n_\downarrow(1-n_\uparrow) + n_\uparrow n_\downarrow &= \mathcal{I}, \\ n_\uparrow n_\downarrow &= n - \mathcal{I}. \end{aligned} \tag{3}$$

Let us consider hopping of a particle to its nearest neighbor site in this reduced Hilbert space. In the full Hilbert space, which does not have the constraint of hole projection, there are four possible nearest neighbor hopping processes as shown in the top panel of Fig. 2. But the only allowed hopping processes in the low-energy Hilbert space of the hole-projected system are those which do not have a hole in the initial state and in which no hole is created in the final state as well. This leaves only one process in which there is a doublon at site j, and a spin $|\sigma\rangle$ at site i. Then a $\bar{\sigma}$ hops from site j to i resulting in a single occupancy at site j and a doublon at site i as shown in the bottom panel of Fig. 2. Thus effectively only hopping of doublons takes place in the projected space resulting in an overall suppression of the hopping process.

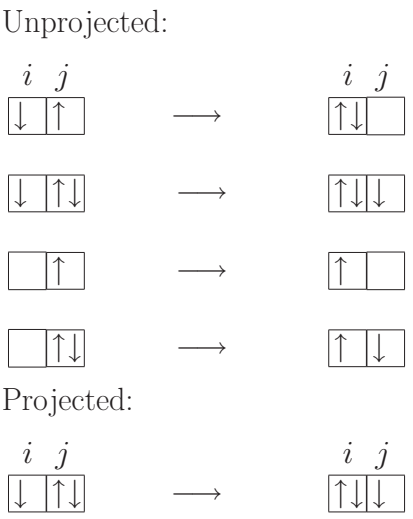

FIG. 2. Top: Possible nearest neighbor hopping process in full Hilbert space. Bottom: Allowed hopping process in reduced Hilbert space from which hole has been projected out.

The corresponding operator for this hopping process is

$$\begin{aligned} H_{\text{hopp}} &= -t \sum_{\langle i,j\rangle,\sigma} X_i^{d\leftarrow\bar{\sigma}} X_j^{\bar{\sigma}\leftarrow d} + \text{H.c.} \\ &= -t \sum_{\langle i,j\rangle,\sigma} \tilde{c}_{i\sigma}^\dagger \tilde{c}_{j\sigma} + \text{H.c.}, \end{aligned} \tag{4}$$

which is equivalently written in terms of normal fermionic operators as

$$\begin{aligned} H_{\text{hopp}} &= -t \sum_{\langle i,j\rangle,\sigma} c_{i\sigma}^\dagger n_{i\bar{\sigma}} n_{j\bar{\sigma}} c_{j\sigma} + \text{H.c.} \\ &= -\mathcal{P}_h \left(t \sum_{\langle i,j\rangle,\sigma} c_{i\sigma}^\dagger c_{j\sigma} + \text{H.c.} \right) \mathcal{P}_h. \end{aligned} \tag{5}$$

Here $\mathcal{P}_h$ stands for the Gutzwiller projection operator for hole projection defined as $\mathcal{P}_h = \prod_i (1-(1-n_{i\uparrow})(1-n_{i\downarrow}))$. We now generalize the concept of the Gutzwiller approximation for hole-projected Hilbert space. The expectation value of the hopping process in the hole-projected Hilbert space can be obtained through the Gutzwiller approximation by renormalizing the hopping term in the unprojected basis by a Gutzwiller factor which takes into account of the physics of projection approximately. The Gutzwiller renormalization factor then is

TABLE I. Probabilities of different states in terms of electron densities in unprojected and hole-projected bases.

States	Unprojected	Projected
$\|\uparrow\rangle$	$\mathbf{n}_\uparrow(1-\mathbf{n}_\downarrow)$	$(1-\mathbf{n}_\downarrow)$
$\|\downarrow\rangle$	$\mathbf{n}_\downarrow(1-\mathbf{n}_\uparrow)$	$(1-\mathbf{n}_\uparrow)$
$\|\uparrow\downarrow\rangle$	$\mathbf{n}_\uparrow\mathbf{n}_\downarrow$	$(\mathbf{n}-1)$
$\|0\rangle$	$(1-\mathbf{n}_\uparrow)(1-\mathbf{n}_\downarrow)$	0

defined as the ratio of the expectation value of an operator O in the projected basis to that in the unprojected basis:

$$g = \frac{\langle\psi|\mathcal{P}_h O \mathcal{P}_h|\psi\rangle}{\langle\psi|O|\psi\rangle}, \tag{6}$$

where ψ is the unprojected state.

The Gutzwiller renormalization factors are determined by the ratios of the probabilities of the corresponding physical processes in the projected and unprojected bases. Listed in Table I are the probabilities of states in unprojected and hole-projected spaces where the spin-resolved unprojected and projected densities have been taken to be equal. Here $\mathbf{n}_\sigma$ is the electron density with spin σ. Consistently everywhere we use $\mathbf{n}$ for density and n for the corresponding number operator.

The probability of hopping of an $\uparrow$-spin electron in the unprojected basis is $(1-\mathbf{n}_{i\uparrow})\mathbf{n}_{j\uparrow}\mathbf{n}_{i\uparrow}(1-\mathbf{n}_{j\uparrow})$. In the hole-projected basis, the corresponding probability is $(\mathbf{n}_j-1)(\mathbf{n}_i-1)(1-\mathbf{n}_{i\uparrow})(1-\mathbf{n}_{j\uparrow})$. Therefore, the Gutzwiller factor for the hopping process comes out to be

$$g_{t\uparrow} = \sqrt{\frac{(\mathbf{n}_i-1)(\mathbf{n}_j-1)}{\mathbf{n}_{i\uparrow}\mathbf{n}_{j\uparrow}}}. \tag{7}$$

With this setup for the hole-projected Hilbert space, we describe the strongly correlated limit of IHM and binary alloys.

III. STRONGLY CORRELATED LIMIT OF IONIC HUBBARD MODEL

IHM has tight-binding electrons on a bipartite lattice (sublattices A and B) described by the Hamiltonian

$$H = -t\sum_{i\in A,j\in B,\sigma}[c^\dagger_{i\sigma}c_{j\sigma}+\text{H.c.}] - \frac{\Delta}{2}\sum_{i\in A}n_i + \frac{\Delta}{2}\sum_{i\in B}n_i + U\sum_i n_{i\uparrow}n_{i\downarrow} - \mu\sum_i n_i. \tag{8}$$

Here t is the nearest neighbor hopping, U the Hubbard repulsion, and Δ a one-body staggered potential which doubles the unit cell. The chemical potential is $\mu = U/2$ for the average occupancy per site to be one, that is, $(\langle n_A\rangle + \langle n_B\rangle)/2 = 1$, corresponding to "half filling".

Let us consider the $t = 0$ limit of this model in the regime $U \sim \Delta$. On the A sublattice, single occupancies have energy $-(\frac{\Delta}{2}+\frac{U}{2}) \sim -\Delta$, the hole has 0 energy, and the doublon has energy $-\Delta$. So, among the four choices of occupancy, a hole on A is the highest energy state and should be projected out from the low-energy Hilbert space. On the other hand, on the B sublattice, single occupancies cost $(\frac{\Delta}{2}-\frac{U}{2}) \sim 0$ energy, holes also cost 0 energy, while doublons cost energy $\Delta \sim U$, and therefore on the B sublattice, doublons should be projected out from the low-energy Hilbert space.

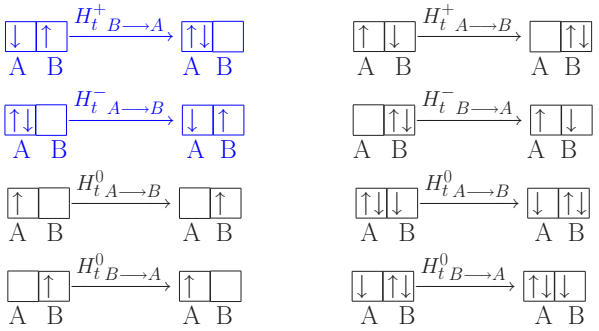

FIG. 3. Nearest neighbor hopping processes for IHM.

A. Low-energy Hamiltonian in the limit $U \sim \Delta \gg t$

In the presence of a nonzero hopping term, the following nearest neighbor processes can take place as shown in Fig. 3. H_t^+ processes involve an increase in double occupancy and hole occupancy by one, H_t^- processes involve a decrease in the double occupancy and hole occupancy by one, and H_t^0 processes involve no change in the double occupancy or hole occupancy. Note that $H^+_{tB\to A}$ and $H^-_{tA\to B}$ are the only processes which are confined to the low-energy sector of the Hilbert space. All other hopping processes mix the high-energy and the low-energy parts of the Hilbert space. The effective low-energy Hamiltonian in the limit $U \sim \Delta \gg t$ can be obtained by doing a similarity transformation which eliminates processes which interconnect the high- and low-energy sectors of the Hilbert space. The effective Hamiltonian is given by

$$\mathcal{H}_{\text{eff}} = e^{iS}He^{-iS} = H + i[S,H] + \frac{i^2}{2}[S,[S,H]] + \cdots. \tag{9}$$

Here S, the transformation operator, is perturbative in t/Δ and $t/(U+\Delta)$ and is given by

$$iS = \frac{1}{U+\Delta}(H_t^+{}_{A\to B} - H_t^-{}_{B\to A}) + \frac{1}{\Delta}\left(H_t^0{}_{A\to B} - H_t^0{}_{B\to A}\right). \tag{10}$$

Higher-order $[O(t^2/U)]$ terms that arise from $[S,H_t]$ and $[S,[S,H_0]]$ and connect the low-energy sector to the high-energy sector can be eliminated by including a second similarity transformation S' such that $[S',H_0]$ cancels those terms. The effective Hamiltonian which does not involve mixing between low- and high-energy subspaces up to order t^2 is

$$\mathcal{H}_{\text{eff}} = H_0 + H_{1,\text{low}} + \frac{1}{U+\Delta}[H_t^+{}_{A\to B}, H_t^-{}_{B\to A}] + \frac{1}{\Delta}\left[H_t^0{}_{A\to B}, H_t^0{}_{B\to A}\right] + O(t^3/U^2)\cdots. \tag{11}$$

Here, $H_0 = U\sum_i n_{i\uparrow}n_{i\downarrow} - \frac{\Delta}{2}\sum_{i\in A}n_i + \frac{\Delta}{2}\sum_{i\in B}n_i$ and $H_{1,\text{low}} = H^+_{tB\to A} + H^-_{tA\to B}$ is the hopping process in the low-energy sector. If we now confine to the low-energy subspace, $\frac{1}{U+\Delta}[H_t^+{}_{A\to B}, H_t^-{}_{B\to A}] \sim -\frac{1}{U+\Delta}H_t^-{}_{B\to A}H_t^+{}_{A\to B}$ because the first term in the commutator demands a doublon at

site B and a hole at site A which is energetically not favorable. Similarly, $\frac{1}{\Delta}[H^0_{t\ A\to B}, H^0_{t\ B\to A}] \sim -\frac{1}{\Delta} H^0_{t\ B\to A} H^0_{t\ A\to B}$ because the first term in the commutator either demands a doublon at B or a hole at A and thus is not allowed because they belong to the high-energy sector.

B. Low-energy Hamiltonian in terms of projected fermions

Since holes on the A sublattice and doublons on the B sublattice belong to the high-energy sector, we have projected them out from the low-energy Hilbert space and introduced new projected operators,

$$\tilde{c}^\dagger_{A\sigma} = \eta(\sigma) X^{d\leftarrow\bar{\sigma}}_A = c^\dagger_{A\sigma} n_{A\bar{\sigma}}, \tag{12}$$

$$\tilde{\tilde{c}}^\dagger_{B\sigma} = X^{\sigma\leftarrow 0}_B = c^\dagger_{B\sigma}(1 - n_{B\bar{\sigma}}). \tag{13}$$

Note that $\{\tilde{\tilde{c}}_\sigma, \tilde{\tilde{c}}^\dagger_\sigma\} = 1 - n_{\bar{\sigma}}$.

While writing in terms of normal fermionic operators in the projected space, the order of the terms in the projected basis becomes important for the A and B sublattices. On the A sublattice, $\tilde{c}_{A\sigma}\tilde{c}^\dagger_{A\sigma} = \mathcal{P}_h c_{A\sigma} c^\dagger_{A\sigma} \mathcal{P}_h$, whereas $\tilde{c}^\dagger_{A\sigma}\tilde{c}_{A\sigma} \neq \mathcal{P}_h c^\dagger_{A\sigma} c_{A\sigma} \mathcal{P}_h$. In the former case, both forms of operators count $\bar{\sigma}$-type single occupancies whereas in the later case $\tilde{c}^\dagger_{A\sigma}\tilde{c}_{A\sigma}$ count double occupancies while $c^\dagger_{A\sigma} c_{A\sigma}$ counts both double occupancies as well as σ-type single occupancies in the hole-projected space. On the B sublattice, the situation is opposite: $\tilde{c}^\dagger_{B\sigma}\tilde{c}_{B\sigma} = \mathcal{P}_d c^\dagger_{B\sigma} c_{B\sigma} \mathcal{P}_d$ and $\tilde{c}_{B\sigma}\tilde{c}^\dagger_{B\sigma} \neq \mathcal{P}_d c_{B\sigma} c^\dagger_{B\sigma} \mathcal{P}_d$. In the former case, both projected and normal fermionic operators count σ-type single occupancies whereas in the latter case the projected space operators count holes while the normal fermionic representation counts holes as well as $\bar{\sigma}$-type single occupancies in the doublon-projected space.

In terms of new projected operators, H_0 in Eq. (11) can be written as $U\sum_{i\in A}(n_i - 1) - \frac{\Delta}{2}[\sum_{i\in A} n_i - \sum_{i\in B} n_i]$. Here we have used that on a site $i \in A$, $n_{i\uparrow} n_{i\downarrow} = n_i - 1$ [see Eq. (3)]. Since doublons have been projected out from the B sublattice, in the low-energy effective Hamiltonian there is no Hubbard term for the B sublattice. The hopping term $H_{1,\text{low}}$ in the projected space does not involve holes on sublattice A and doublons on sublattice B. The representation in terms of projected operators is

$$\begin{aligned} H_{1,\text{low}} &= -t \sum_{\langle ij\rangle,\sigma} \tilde{c}^\dagger_{iA\sigma}\tilde{\tilde{c}}_{jB\sigma} + \tilde{\tilde{c}}^\dagger_{jB\sigma}\tilde{c}_{iA\sigma} \\ &= -t \sum_{\langle ij\rangle,\sigma} \mathcal{P}[c^\dagger_{iA\sigma} c_{jB\sigma} + \text{H.c.}]\mathcal{P}. \end{aligned} \tag{14}$$

Here the projection operator $\mathcal{P}$ projects out holes from the Hilbert space corresponding to sublattice A and doublons from the Hilbert space on sublattice B.

$O(t^2/(U+\Delta))$ *dimer terms*. In terms of Hubbard operators, the dimer term corresponding to $\frac{1}{U+\Delta}[H^+_{t\ A\to B}, H^-_{t\ B\to A}] \sim -\frac{1}{U+\Delta} H^-_{t\ B\to A} H^+_{t\ A\to B}$ becomes

$$H^1_{\text{dimer}} = -\frac{t^2}{U+\Delta} \sum_{i\in A, j\in B,\sigma} \left[X^{\sigma\leftarrow\sigma}_i X^{\bar{\sigma}\leftarrow\bar{\sigma}}_j - X^{\bar{\sigma}\leftarrow\sigma}_i X^{\sigma\leftarrow\bar{\sigma}}_j\right].$$

The corresponding process is represented in Fig. 4. In terms of projected fermionic operators, these dimer terms take the following form:

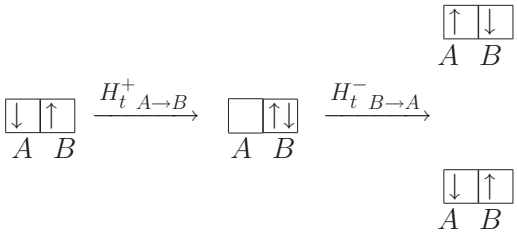

FIG. 4. Spin exchange and spin preservation dimer terms for IHM.

$$\begin{aligned} &= -\frac{t^2}{U+\Delta} \sum_{i,j,\sigma} [\tilde{c}_{iA\bar{\sigma}}\tilde{c}^\dagger_{iA\bar{\sigma}}\tilde{\tilde{c}}^\dagger_{jB\bar{\sigma}}\tilde{\tilde{c}}_{jB\bar{\sigma}} - \tilde{c}_{iA\sigma}\tilde{c}^\dagger_{iA\bar{\sigma}}\tilde{\tilde{c}}^\dagger_{jB\sigma}\tilde{\tilde{c}}_{jB\bar{\sigma}}] \\ &= J_1 \sum_{i,j} \mathcal{P}[S_{iA}\cdot S_{jB} - (2 - n_{iA})n_{jB}/4]\mathcal{P} \end{aligned} \tag{15}$$

with $J_1 = \frac{2t^2}{U+\Delta}$. Projection operator $\mathcal{P}$ projects out hole from sublattice A and doublons from sublattice B. Note that in writing the above renormalized form of the Heisenberg part of the Hamiltonian, we have imposed SU(2) symmetry by hand [7,32]. Within the simplest approximation of spin-resolved densities being same in projected and unprojected states, the Gutzwiller approximation factor for $S^z_{iA}S^z_{jB}$ remains unity while the Gutzwiller factor for the $S^+_{iA}S^-_{jB} + \text{H.c.}$ term is g_s. Since the original Hamiltonian is SU(2) symmetric, the renormalized Hamiltonian obtained after taking into account the effect of projection must also be SU(2) symmetric. Hence we used g_s to be the Gutzwiller factor for the $S^z_{iA}S^z_{jB}$ term as well.

The dimer term corresponding to $[H^0_{t\ A\to B}, H^0_{t\ B\to A}]$ involves hopping of an electron or a doublon from some site to its nearest neighbor site and back to the initial site as shown in Fig. 5. This process is of order t^2/Δ and can be written as

$$H^2_{\text{dimer}} = -\frac{t^2}{\Delta} \sum_{\sigma,\langle ij\rangle} \left[X^{\sigma\leftarrow\sigma}_{iA} X^{0\leftarrow 0}_{jB} + X^{d\leftarrow d}_{iA} X^{\bar{\sigma}\leftarrow\bar{\sigma}}_{jB}\right].$$

In terms of projected operators we get

$$\begin{aligned} &= -\frac{t^2}{\Delta} \sum_{\sigma,\langle ij\rangle} [\tilde{c}_{iA\bar{\sigma}}\tilde{c}^\dagger_{iA\bar{\sigma}}\tilde{\tilde{c}}_{jB\sigma}\tilde{\tilde{c}}^\dagger_{jB\sigma} + \tilde{c}^\dagger_{iA\sigma}\tilde{c}_{iA\sigma}\tilde{\tilde{c}}^\dagger_{jB\bar{\sigma}}\tilde{\tilde{c}}_{jB\bar{\sigma}}] \\ &= -\frac{t^2}{\Delta} \sum_{\langle ij\rangle,\sigma} \mathcal{P}[(1 - n_{iA\bar{\sigma}})(1 - n_{jB}) + (n_{iA} - 1)n_{jB\bar{\sigma}}]\mathcal{P}. \end{aligned} \tag{16}$$

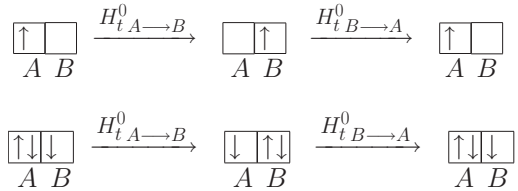

FIG. 5. Top: Hopping of a single spin to site B and back to site A. Bottom: Hopping of a doublon from A to B and back to A.

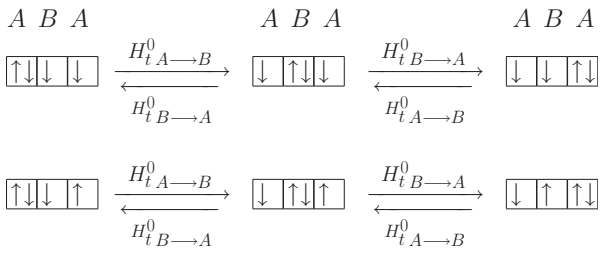

FIG. 6. Effective next nearest neighbor hopping of a doublon within A sublattice.

$O(t^2/\Delta)$ *trimer terms*. Trimer terms involve hopping of a doublon or a hole from a site to its next nearest neighbor site. Effectively there is doublon hopping which is intra-A-sublattice hopping denoted by H^{AA}_{hopp} whereas the hole hopping is intra-B-sublattice hopping (H^{BB}_{hopp}) as shown in Figs. 6 and 7.

In terms of X operators, hopping processes for doublon hopping, which is of $O(t^2/\Delta)$, on the A sublattice are represented as

$$H^{AA}_{\text{hopp}} = -\frac{t^2}{\Delta}\sum_{\sigma,\langle ijk\rangle} X^{d\leftarrow\bar\sigma}_{kA} X^{\bar\sigma\leftarrow\bar\sigma}_{jB} X^{\bar\sigma\leftarrow d}_{iA} + X^{d\leftarrow\sigma}_{kA} X^{\sigma\leftarrow\bar\sigma}_{jB} X^{\bar\sigma\leftarrow d}_{iA} + \text{H.c.}$$

In terms of projected operators, they are represented as

$$= -\frac{t^2}{\Delta}\sum_{\sigma,\langle ijk\rangle} (\tilde c^\dagger_{kA\sigma}\tilde{\tilde c}^\dagger_{jB\bar\sigma}\tilde{\tilde c}_{jB\bar\sigma}\tilde c_{iA\sigma} + \tilde c_{iA\bar\sigma}\tilde{\tilde c}^\dagger_{jB\bar\sigma}\tilde{\tilde c}_{jB\sigma}\tilde c^\dagger_{kA\sigma})$$

$$= -\frac{t^2}{\Delta}\sum_{\sigma,\langle ijk\rangle} \mathcal{P}(c^\dagger_{kA\sigma} n_{jB\bar\sigma} c_{iA\sigma} + c_{iA\bar\sigma} c^\dagger_{jB\bar\sigma} c_{jB\sigma} c^\dagger_{kA\sigma})\mathcal{P}. \tag{17}$$

Similarly the hopping of holes within the B sublattice, shown in Fig. 7, can be written in terms of X operators as

$$H^{BB}_{\text{hopp}} = -\frac{t^2}{\Delta}\sum_{\sigma,\langle jil\rangle} X^{0\leftarrow\sigma}_{lB} X^{\sigma\leftarrow\sigma}_{iA} X^{\sigma\leftarrow 0}_{jB} + X^{0\leftarrow\bar\sigma}_{lB} X^{\bar\sigma\leftarrow\sigma}_{iA} X^{\sigma\leftarrow 0}_{jB} + \text{H.c.},$$

which can be written in terms of projected operators as

$$= -\frac{t^2}{\Delta}\sum_{\sigma,\langle jil\rangle} (\tilde{\tilde c}_{lB\sigma}\tilde c_{iA\bar\sigma}\tilde c^\dagger_{iA\bar\sigma}\tilde{\tilde c}^\dagger_{jB\sigma} + \tilde{\tilde c}^\dagger_{jB\sigma}\tilde c_{iA\sigma}\tilde c^\dagger_{iA\bar\sigma}\tilde{\tilde c}_{lB\bar\sigma})$$

$$= -\frac{t^2}{\Delta}\sum_{\sigma,\langle jil\rangle} \mathcal{P}\{c_{lB\sigma}[(1-n_{iA\bar\sigma})c^\dagger_{jB\sigma} + c^\dagger_{iA\sigma}c_{iA\bar\sigma}c^\dagger_{jB\bar\sigma}]\}\mathcal{P}. \tag{18}$$

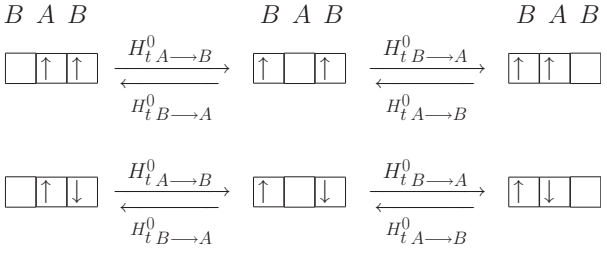

FIG. 7. Effective next nearest neighbor hopping of hole for IHM.

C. Gutzwiller approximation

The effective low-energy Hamiltonian obtained in the above section can be written as $\mathcal{H}_{\text{eff}} = \mathcal{P}\tilde H\mathcal{P}$ where $\mathcal{P}$ will project out holes from the A sublattice and doublons from the B sublattice for half filling and densities close to half filling. Within the Gutzwiller approximation, the effect of this projection is taken approximately by renormalizing various coupling terms in $\tilde H$ by corresponding Gutzwiller factors such that eventually the expectation value of the renormalized Hamiltonian can be calculated in the normal basis. Further we will calculate the Gutzwiller approximation factors under the assumption that the spin-resolved densities before and after the projection remain the same which will make Gutzwiller factors equal to 1 for some terms in $\tilde H$. The renormalized Hamiltonian can be written as

$$\begin{aligned}\tilde H = H_0 &- t\sum_{\sigma,\langle ij\rangle} g_{t\sigma}[c^\dagger_{iA\sigma}c_{jB\sigma} + \text{H.c.}] \\ &- \frac{t^2}{\Delta}\sum_{\langle ij\rangle,\sigma}[g_1(1-n_{iA\bar\sigma})(1-n_{jB}) + g_2(n_{iA}-1)n_{jB\bar\sigma}] \\ &- \frac{t^2}{\Delta}\sum_{\sigma,\langle ijk\rangle}(g_{3\sigma}c^\dagger_{kA\sigma}n_{jB\bar\sigma}c_{iA\sigma} + g_4 c_{iA\bar\sigma}c^\dagger_{jB\bar\sigma}c_{jB\sigma}c^\dagger_{kA\sigma}) \\ &+ \text{H.c.} - \frac{t^2}{\Delta}\sum_{\sigma,\langle jil\rangle}[g_{5\sigma}c_{lB\sigma}(1-n_{iA\bar\sigma})c^\dagger_{jB\sigma} \\ &+ g_6 c_{lB\sigma}c^\dagger_{iA\sigma}c_{iA\bar\sigma}c^\dagger_{jB\bar\sigma}] + \text{H.c.} \\ &+ \frac{2t^2}{U+\Delta}\sum_{\langle i,j\rangle}\left[g_s S_{iA}\cdot S_{jB} - \frac{1}{4}(2-n_{iA})n_{jB}\right].\end{aligned} \tag{19}$$

Here $g_{t,\sigma}$ and g_s are Gutzwiller approximation factors for the nearest neighbor hopping and spin exchange terms. g_1 and g_2 are Gutzwiller factors for dimer terms $H^{1,2}_{\text{dimer}}$, respectively. $g_{3\sigma}$ and g_4 are Gutzwiller factors for intra-sublattice hopping of doublons on the A sublattice and $g_{5,\sigma}$ and g_6 are Gutzwiller factors for the intra-sublattice hopping of holes on B sublattice. As we will demonstrate, some of the Gutzwiller factors are spin symmetric while others might be spin dependent in a spin-symmetry-broken phase like in antiferromagnetically ordered phases. Below we evaluate them one by one for various processes involved in $\mathcal{H}_{\text{eff}}$. We have listed below in Table II the probabilities of different states in the doublon-projected basis. Probabilities for various states for the hole-projected sublattice were listed in Table I.

As we mentioned earlier, this analysis holds at half filling and for densities not far from half filling. Even if the system

TABLE II. Probabilities of different states in terms of electron densities in unprojected and doublon-projected bases.

States	Unprojected	Projected
$\lvert\uparrow\rangle$	$\mathbf{n}_\uparrow(1-\mathbf{n}_\downarrow)$	$\mathbf{n}_\uparrow$
$\lvert\downarrow\rangle$	$\mathbf{n}_\downarrow(1-\mathbf{n}_\uparrow)$	$\mathbf{n}_\downarrow$
$\lvert\uparrow\downarrow\rangle$	$\mathbf{n}_\uparrow\mathbf{n}_\downarrow$	0
$\lvert 0\rangle$	$(1-\mathbf{n}_\uparrow)(1-\mathbf{n}_\downarrow)$	$(1-\mathbf{n})$

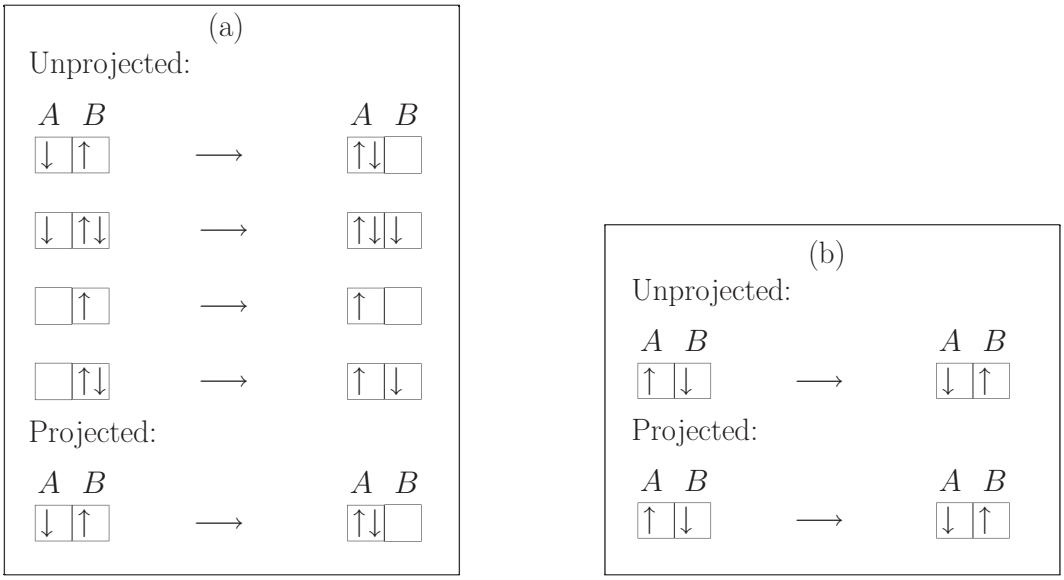

FIG. 8. (a) Processes involved in the calculation of nearest neighbor hopping renormalization factor, $g_{t,\sigma}$. (b) Processes involved in the calculation of spin exchange renormalization factor g_s.

is overall half filled, the individual sublattices are not; the A sublattice is electron doped whereas the B sublattice is hole doped. At half filling in the Hubbard model, the Gutzwiller renormalization factor for hopping is zero because the system is an antiferromagnetic Mott insulator whereas in the case of IHM, the density difference between the sublattices results in finite $g_{t,\sigma}$. Here, as we will show, the density difference between two sublattices plays the role of doping in the case of the Hubbard model. Also, the trimer terms are present in the half-filled IHM which results in intra-sublattice hopping of holes and doublons whereas the half-filled Hubbard model has no trimer terms.

Below we first give the general expression for $g_{t,\sigma}$ and g_s at any filling and then evaluate them for the special case of half filling, $\frac{\mathbf{n}_A+\mathbf{n}_B}{2}=1$. The probability of nearest neighbor hopping of an $\uparrow$ electron in the unprojected space (shown in Fig. 8) is $(1-\mathbf{n}_{A\uparrow})\mathbf{n}_{B\uparrow}\mathbf{n}_{A\uparrow}(1-\mathbf{n}_{B\uparrow})$ and in the unprojected space it is $(1-\mathbf{n}_{A\uparrow})\mathbf{n}_{B\uparrow}(\mathbf{n}_A-1)(1-\mathbf{n}_B)$. Then, the Gutzwiller renormalization factor

$$g_{t\uparrow}=\sqrt{\frac{(\mathbf{n}_A-1)(1-\mathbf{n}_B)}{\mathbf{n}_{A\uparrow}(1-\mathbf{n}_{B\uparrow})}}. \tag{20}$$

Let $\delta=\frac{\mathbf{n}_A-\mathbf{n}_B}{2}$ be the density difference between two sublattices. Then at half filling, the density of the A sublattice is $\mathbf{n}_A=1+\delta$ and that of the B sublattice is $\mathbf{n}_B=1-\delta$. Let the magnetization on the A sublattice $m_A=\mathbf{n}_{A\uparrow}-\mathbf{n}_{A\downarrow}$; then at half filling due to particle-hole symmetry, $m_A=-m_B=m$. One can rewrite $g_{t,\sigma}=\frac{2\delta}{1+\delta+\sigma m}$ in an antiferromagnetically ordered phase at half filling. For $m=0$, g_t takes a form similar to that known for the doped t-J model with δ, the density difference in IHM, playing the role of hole doping in the t-J model.

Now consider the spin exchange process shown in Fig. 8(b). The probability for this process to take place in the unprojected basis is $\mathbf{n}_{A\uparrow}(1-\mathbf{n}_{A\downarrow})\mathbf{n}_{B\downarrow}(1-\mathbf{n}_{B\uparrow})\mathbf{n}_{A\downarrow}(1-\mathbf{n}_{A\uparrow})\mathbf{n}_{B\uparrow}(1-\mathbf{n}_{B\downarrow})$, whereas in the projected basis it is $(1-\mathbf{n}_{A\downarrow})\mathbf{n}_{B\downarrow}(1-\mathbf{n}_{A\uparrow})\mathbf{n}_{B\uparrow}$, resulting in the Gutzwiller factor

$$g_s=\sqrt{\frac{1}{\mathbf{n}_{A\uparrow}\mathbf{n}_{A\downarrow}(1-\mathbf{n}_{B\uparrow})(1-\mathbf{n}_{B\downarrow})}}. \tag{21}$$

Again at half filling in an AFM ordered phase $g_s=4/[(1+\delta)^2-m^2]$ which for $m=0$ again maps to the g_s factor for the doped t-J model with δ playing the role of hole doping in that case.

The Gutzwiller factors g_1, g_2 are 1 because the dimer terms $H^{1,2}_{\text{dimer}}$ are the products of densities. Under the assumption that the spin-resolved unprojected and projected densities are the same, the Gutzwiller factors for these terms are 1.

Now we will calculate Gutzwiller factors for various trimer terms shown in Fig. 6 and Fig. 7. Figure 9(a) shows hopping of an $\uparrow$ electron within the A sublattice with a spin $\downarrow$ on the intermediate B site being preserved. In the unprojected basis, the probability for this process to happen is $\mathbf{n}^2_{A\uparrow}(1-\mathbf{n}_{A\uparrow})^2\mathbf{n}^2_{B\downarrow}$. It is to be noted that processes with either a down-type particle or a doublon at the intermediate B site have been considered in the unprojected space. Likewise, the probability for the process to happen in the projected basis is $(\mathbf{n}_A-1)^2(1-\mathbf{n}_{A\uparrow})^2\mathbf{n}^2_{B\downarrow}$. Therefore, the Gutzwiller factor for this process is

$$g_{3\uparrow}=\frac{\mathbf{n}_A-1}{\mathbf{n}_{A\uparrow}}=\frac{2\delta}{1+\delta+m}, \tag{22}$$

where the expression on the rightmost side holds in the case of half filling for nonzero staggered magnetization. In general one gets $g_{3\sigma}=\frac{\mathbf{n}_A-1}{\mathbf{n}_{A\sigma}}$. Figure 9(b) depicts hopping processes on the A sublattice in which spin on the intermediate B site gets flipped. The probability in the unprojected basis for this process to occur is $(1-\mathbf{n}_{A\uparrow})(1-\mathbf{n}_{A\downarrow})\mathbf{n}_{A\uparrow}\mathbf{n}_{A\downarrow}(1-\mathbf{n}_{B\uparrow})(1-\mathbf{n}_{B\downarrow})\mathbf{n}_{B\uparrow}\mathbf{n}_{B\downarrow}$ whereas that in the projected basis is $(\mathbf{n}_A-1)^2(1-\mathbf{n}_{A\uparrow})(1-\mathbf{n}_{A\downarrow})\mathbf{n}_{B\uparrow}\mathbf{n}_{B\downarrow}$ resulting in the Gutzwiller

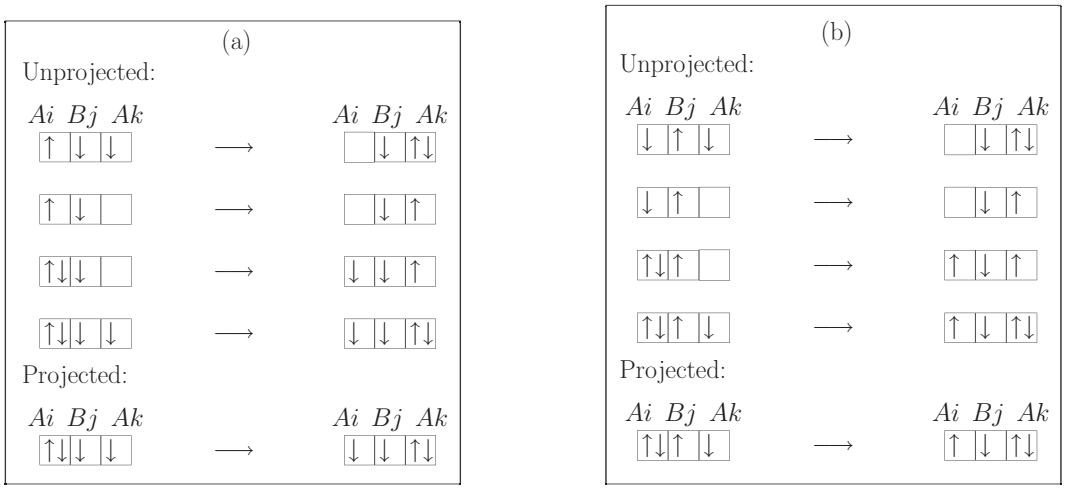

FIG. 9. (a) Processes involved in the calculation of g_3. Similar physical processes with doublon at B site in the unprojected basis are considered in the calculation (but not shown here). (b) Processes involved in the calculation of g_4.

factor

$$g_4 = \frac{\mathbf{n}_A - 1}{\sqrt{\mathbf{n}_{A\uparrow}\mathbf{n}_{A\downarrow}(1-\mathbf{n}_{B\uparrow})(1-\mathbf{n}_{B\downarrow})}} = \frac{4\delta}{(1+\delta)^2 - m^2}. \tag{23}$$

Now consider the hopping processes within the B sublattice depicted in Fig. 7. Figure 10(a) shows hopping of an $\uparrow$-spin particle within the B sublattice such that spin on the intermediate A site is preserved. Here again it must be noted that processes with either an up particle or a hole at the intermediate A site have been considered in the unprojected basis. In the unprojected basis the probability of this process is $(1-\mathbf{n}_{A\downarrow})^2\mathbf{n}_{B\uparrow}^2(1-\mathbf{n}_{B\uparrow})^2$ and that in the projected basis is $(1-\mathbf{n}_{A\downarrow})^2\mathbf{n}_{B\uparrow}^2(1-\mathbf{n}_B)^2$ leading to the Gutzwiller factor

$$g_{5\uparrow} = \frac{1-\mathbf{n}_B}{1-\mathbf{n}_{B\uparrow}} = \frac{2\delta}{1+\delta+m}. \tag{24}$$

In general, $g_{5,\sigma} = (1-\mathbf{n}_B)/(1-\mathbf{n}_{B\sigma})$ is spin dependent.

Another hopping process within the B sublattice is the one in which spin on the intermediate A site gets flipped. The probability for this process to occur in the unprojected basis is $(1-\mathbf{n}_{A\uparrow})(1-\mathbf{n}_{A\downarrow})\mathbf{n}_{A\uparrow}\mathbf{n}_{A\downarrow}(1-\mathbf{n}_{B\uparrow})(1-\mathbf{n}_{B\downarrow})\mathbf{n}_{B\uparrow}\mathbf{n}_{B\downarrow}$ and in the projected space it is $(1-\mathbf{n}_{A\uparrow})(1-\mathbf{n}_{A\downarrow})\mathbf{n}_{B\uparrow}\mathbf{n}_{B\downarrow}(1-\mathbf{n}_B)^2$. The Gutzwiller factor is therefore

$$g_6 = \frac{1-\mathbf{n}_B}{\sqrt{\mathbf{n}_{A\uparrow}\mathbf{n}_{A\downarrow}(1-\mathbf{n}_{B\uparrow})(1-\mathbf{n}_{B\downarrow})}} = \frac{4\delta}{(1+\delta)^2 - m^2}. \tag{25}$$

D. Results for strongly correlated limit of IHM

In this section we present results for the IHM in the limit $U \sim \Delta \gg t$ at half filling. To be specific, we do mean field decomposition of the renormalized low-energy Hamiltonian in Eq. (19) giving nonzero expectation values to the following mean fields: (i) magnetization on the A sublattice (B sublattice), m_A (m_B); (ii) inter-sublattice Fock shift (χ_{AB}); (iii) intra-

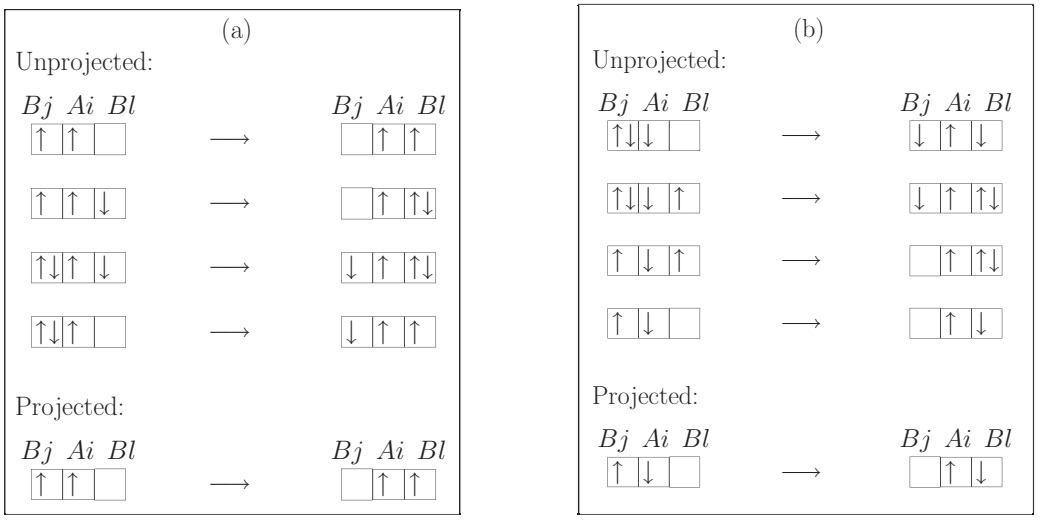

FIG. 10. (a) Processes involved in the calculation of g_5. Similar physical processes with hole at A site in the unprojected basis are considered in the calculation of g_5 (but not shown here). (b) Processes involved in the calculation of g_6.

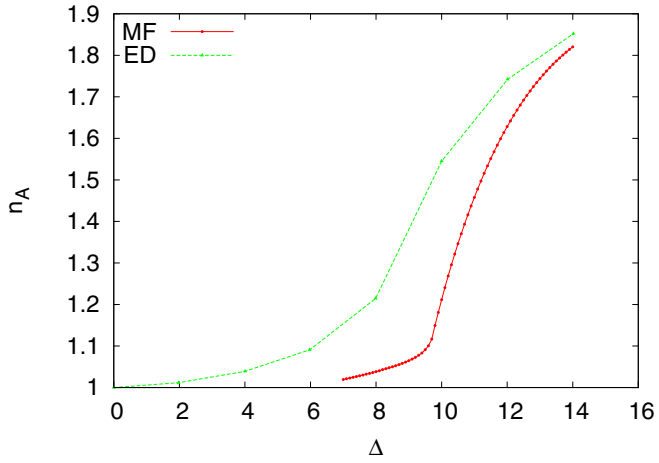

FIG. 11. Density on sublattice A as a function of Δ for $U = 10t$. ED results shown are obtained from [33].

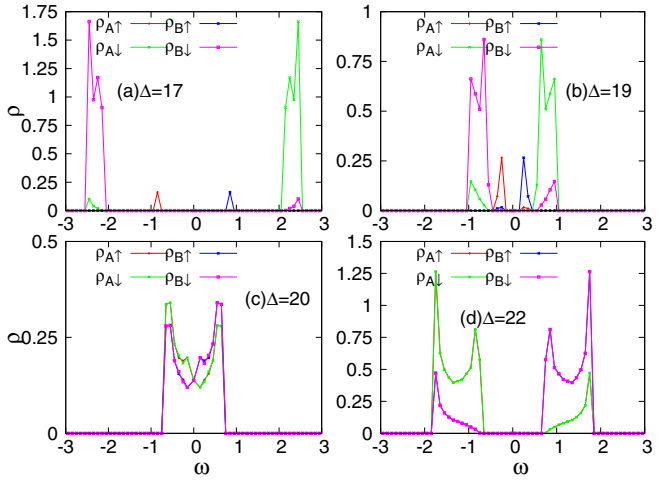

FIG. 12. Single-particle DOS for $U = 20t$ for a few values of Δ. For $\Delta < U$, the system has spin asymmetry with $\rho_{\alpha\uparrow}(\omega) \neq \rho_{\alpha\downarrow}(\omega)$. Also the gap in the DOS is larger for the down-spin channel. As Δ increases towards U, both the gaps decrease eventually giving a metallic phase for $\Delta \sim U$. As Δ increases further again the system becomes an insulator which has spin symmetry.

sublattice Fock shifts; (iv) Hartree shifts; and (v) the density difference between the two sublattices (δ). The quadratic mean field Hamiltonian is solved by appropriate canonical transformation and mean fields are obtained self-consistently. Below we first provide a comparison of our approach with the results obtained from an exact diagonalization (ED) study of this model for a one-dimensional chain followed up by the results towards a possible phase diagram of the IHM in the limit of validity of this approach.

1. Comparison with ED results

Below we first benchmark our approach of hole and doublon projection, implemented at the level of the renormalized low-energy Hamiltonian via the Gutzwiller approximation, by comparing our results for a 1d chain with those obtained from exact diagonalization by Anusooya-Pati *et al.* [33]. Since the formalism we have developed in this paper is valid for the regime of both U and Δ being much larger than the hopping amplitude t we compare our results for the largest value of U for which results are shown in [33]. Figure 11 shows the density on sublattice A as a function of Δ for $U = 10t$ for a 1d chain. The ED result, obtained by digitizing the plot from the work of Anusooya-Pati *et al.* [33], is an extrapolation of finite-size chains in the thermodynamic limit. For smaller values of Δ our formalism does not hold and hence the comparison has been shown for $\Delta \geqslant 7t$. The qualitative trend in both the calculations is the same and as Δ increases better quantitative consistency is observed between the two calculations. Note that there is an overall factor of 2 difference in the ionic potential term in our Hamiltonian and the one used in Anusooya-Pati *et al.* After this checks to validate our formalism, we provide below the details of the phase diagram of IHM in the limit under consideration.

2. Phase diagram of IHM for $U \sim \Delta \gg t$

The phase diagram of IHM in the limit $U \sim \Delta \gg t$ has not been explored in detail so far. There are a few numerical results available [16,33] but a complete understanding has been lacking mainly because no perturbative calculation has been developed in this limit so far. One of the reasons is that the formalism for hole projection, which is essential in this limit, was missing so far in the literature. Below we provide details of various physical quantities based on the mean field analysis of our renormalized Hamiltonian for a 1d chain and also discuss possible phases in higher-dimensional cases.

Single-particle density of states. In this section we discuss the single-particle density of states (DOS) $\rho_{\alpha\sigma}(\omega) \equiv -\sum_k \mathrm{Im}\, \hat{G}_{\alpha\sigma}(k,\omega^+)/\pi$. Here α represents the sublattice A,B and σ is the spin. In the Gutzwiller approximation, we must rescale the Green's function $G_{\alpha\sigma}(k,\omega)$ with the correct Gutzwiller factor [32] just like we did for hopping, spin exchange, and trimer terms in the Hamiltonian. Thus the renormalized $G_{\alpha\sigma}(k,\omega) = g_{t,\sigma} G^0_{\alpha\sigma}(k,\omega)$ where $G^0_{\alpha\sigma}(k,\omega)$ is the Green's functions calculated in the unprojected ground state of the Hamiltonian in Eq. (19). The corresponding spectral function which is the imaginary part of the Green's function also satisfies the relation $A_{\alpha\sigma}(k,\omega) = g_{t\sigma} A^0_{\alpha\sigma}(k,\omega)$ resulting in the same relation for the single-particle density of states $\rho_{\alpha\sigma}(\omega)$. Figure 12 shows the renormalized single-particle DOS in the projected Hilbert space for the IHM for $U = 20t$ and a few values of $\Delta \sim U$. For $\Delta < \Delta_c$, the system has spin asymmetry as seen in the top two panels of Fig. 12. There is a gap in the DOS for both the up- and the down-spin channels, with gap in the up-spin channel being smaller than that for the down-spin channel. Both the gaps reduce with increase in Δ as shown in panels (b) and (c) of Fig. 12 eventually becoming vanishingly small for a range of Δ values close to $\Delta = U$ where the system is metallic. On further increasing Δ, the gap in the DOS opens up again but now the system is spin symmetric with both the gaps being equal. Figure 13 shows the behavior of gap_σ as a function of Δ for $U = 20t$.

The existence of a metallic phase intervening between the two insulating phases of the IHM has been a debatable issue in the literature. Though the solution of DMFT self-consistent equations in the paramagnetic (PM) sector at half filling at

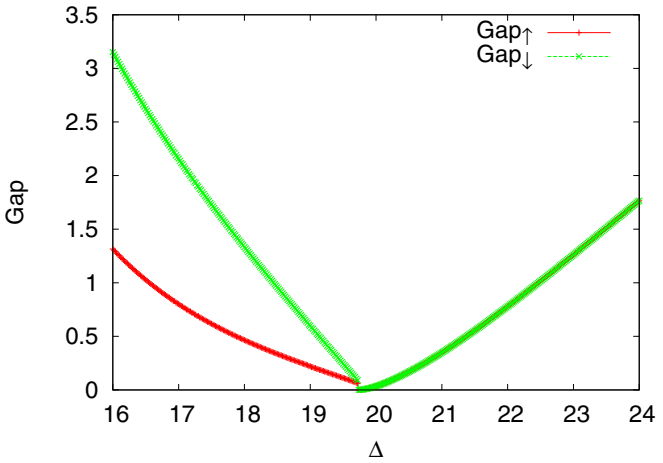

FIG. 13. The gap in the single-particle density of states vs Δ for $U = 20$. For $\Delta < U$, $gap_\downarrow > gap_\uparrow$ and both decrease with increase in Δ eventually becoming zero for $\Delta \sim U$. As Δ increases further, the gap opens up again but the gaps in the up and down channels are equal in this phase.

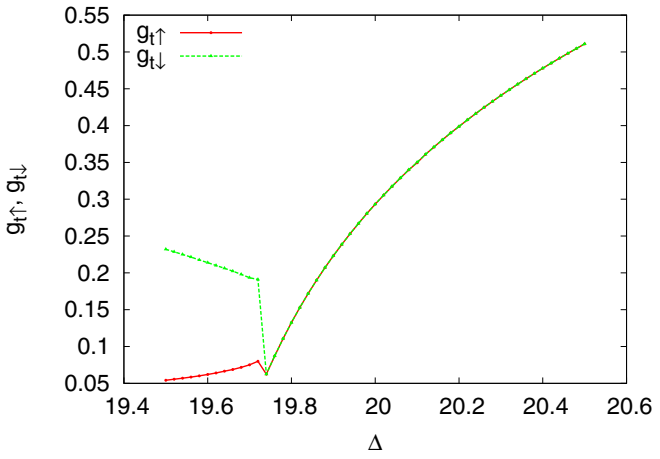

FIG. 14. Plot of $g_{t\sigma}$ vs Δ for $U = 20$. In the metallic phase $g_{t\sigma}$ provides the quasiparticle weight.

zero temperature shows an intervening metallic phase [10], in the spin-asymmetric sector, the transition from paramagnetic band insulator (PM BI) to antiferromagnetic (AFM) insulator preempts the formation of a parametallic phase [12,19]. But determinantal quantum Monte Carlo results demonstrated the presence of a metallic phase even in the spin-asymmetric solution [17,18]. Exact diagonalization for 1d chains [33] has also shown signatures of the presence of a metallic phase via calculation of the charge stiffness. In all the cases, where an intervening metallic phase has been demonstrated, it was also shown that the width of the metallic phase shrinks with increase in U and Δ. A very narrow metallic regime observed in our approach for the IHM at half filling for $U \sim \Delta \gg t$ is completely consistent with these studies.

The renormalized momentum distribution function $n_{\alpha\sigma}(k) = \int d\omega A_{\alpha\sigma}(k,\omega) = g_{t\sigma} n^0_{\alpha\sigma}(k)$, where $n^0_{\alpha\sigma}(k)$ is the momentum distribution function in the unprojected Hilbert space. Thus the quasiparticle weight, which is the jump in the momentum distribution function at the Fermi momentum, is $Z = g_{t\sigma}$. Figure 14 shows $g_{t\sigma}$ vs Δ for $U = 20t$. In the metallic regime, that is, for $\Delta \sim 20t$, $g_{t\uparrow} = g_{t\downarrow} \ll 1$ which indicates that we actually have a *bad* metal, with very heavy quasiparticles, intervening between the two insulators. Note that in the insulating regime $g_{t\sigma}$ does not carry the meaning of quasiparticle weight.

Magnetization and staggered density. The staggered magnetization m, defined as $m = (m_A - m_B)/2$, calculated within the renormalized mean field theory is shown in Fig. 15. For a given $U \gg t$, $m = 0$ for $\Delta > U$ but as Δ approaches U, the antiferromagnetic order sets in with a jump in m at Δ_c. As Δ decreases further, m increases approaching the saturation value. Note that for very small values of Δ where m might tend to unity, our approach does not work.

The staggered density difference $\delta = (n_A - n_B)/2$ is shown in the green curve in Fig. 15 as a function of Δ. As expected for $\Delta > U$, δ is large close to its saturation value and with decrease in Δ, δ reduces monotonically for $\Delta > \Delta_c$. At Δ_c, there occurs a change in slope $\frac{\partial\delta}{\partial\Delta}$. Note that within our approach the system can never attain the saturation values $m = 1$ and $\delta = 0$ at which the Gutzwiller factor for the spin exchange term g_s diverges and the perturbation theory fails.

Possible superconductivity in higher dimensions. Based on the renormalized Hamiltonian in Eq. (19) one can see that even at half filling for the overall lattice, there is a finite hopping between A and B sublattices in the projected space as long as the density difference δ is nonzero. This effectively gives a doped t-J model for each sublattice even at half filling. Further there are finite next nearest neighbor hopping terms within each sublattice which appear through trimer terms in the Hamiltonian in Eq. (19). In this renormalized Hamiltonian there is a possibility that the metallic phase mentioned above can turn into a d-wave superconducting phase or $d + is$ pairing superconducting phase in higher-dimensional systems. The superconducting phase might survive for a larger range of U-Δ space compared to the metallic phase with support of trimer terms. This will be explored in future work.

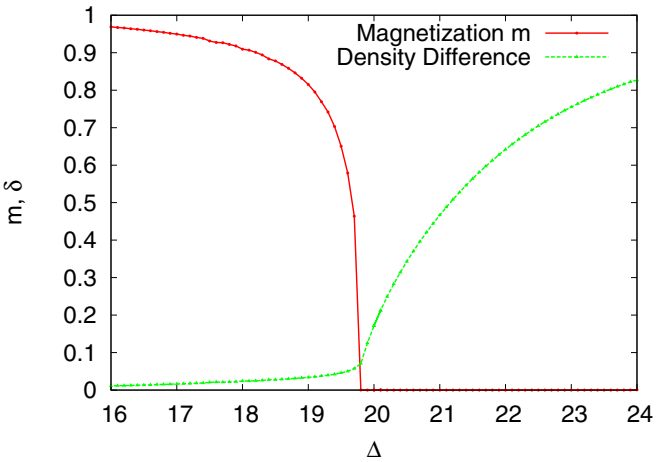

FIG. 15. Staggered magnetization m and staggered density δ vs Δ for $U = 20t$. At $\Delta_c \sim 19.8t$, m drops to zero with a discontinuity. At the same point a discontinuity is seen in the slope $\frac{\partial\delta}{\partial\Delta}$.

Possible half-metal phase. Depending upon the dimensionality of the problem and the lattice structure, it might be easier to frustrate the antiferromagnetic order with the help of trimer terms of Hamiltonian in Eq. (19). The overall strength of the coefficient of various trimer terms is a nonmonotonic function of Δ. In the regime $\Delta \sim U$ where the staggered density difference is finite, effective next nearest neighbor hopping obtained from Fock shift decomposition of these terms might become significant and start competing with the nearest neighbor hopping term. In this case even at half filling the effective low-energy Hamiltonian does not have particle-hole symmetry and $m_A \neq -m_B$. Rather than having just nonzero staggered magnetization $m = (m_A - m_B)/2$, there might be a nonzero uniform magnetization $m_F = (m_A + m_B)/2$ as well resulting in the ferrimagnetic order for $\Delta \sim U$. Further due to different gaps in the single-particle DOS for up- and down-spin channels, there is a possibility that the half-metallic phase appears as a precursor to the metallic phase mentioned above. A similar mechanism for half metal has been seen in the doped IHM [13] for weak to intermediate strength of U and Δ where particle-hole symmetry is broken explicitly by adding holes into the system while in the extremely correlated limit presented in this work, trimer terms can break the particle-hole symmetry spontaneously.

Nonmonotonic behavior of Néel temperature with Δ. The renormalized Hamiltonian in Eq. (19) is illuminating enough to predict the behavior of the Néel temperature for the AFM order in the IHM in the large U and Δ regime at half filling. For $U \gg t$ but $\Delta \sim t$, the IHM maps to the modified t-J model with an additional ionic potential term and with the spin-exchange term given by $\tilde{J} = 4t^2U/(U^2 - \Delta^2)$ [16]. Note that in this limit doublons are projected out from the low-energy Hilbert space from all sites. In this case the Néel temperature of the AFM order should obey $\tilde{J}$ and hence increase as Δ increases. In fact this was observed in DMFT+CTQMC calculation for the IHM at half filling [16] where it was shown that for U as high as $16t$, up to Δ little less than U, $T_N \sim \tilde{J}/4$ [34]. But for $\Delta \geqslant U$ a sudden drop in T_N was observed which could not be explained based on the spin exchange coupling $\tilde{J}$.

Our current renormalized Hamiltonian sheds light on this nonmonotonic behavior of T_N since it is valid for the $U \sim \Delta$ as well as for the $\Delta > U$ regime. In this regime the coefficient of spin exchange term is $\tilde{\tilde{J}} = 2t^2/(U + \Delta)$ which decreases with increase in Δ. Hence for $U \gg t$, for small values of $\Delta \leqslant U$, T_N follows $\tilde{J}$ and hence T_N increases with Δ. As Δ increases further T_N starts to follow the new coupling $\tilde{\tilde{J}}$ and starts decreasing with increase in Δ.

To summarize, in the strongly correlated limit of the ionic Hubbard model, the interplay of U and Δ promises a rich phase diagram, and our formalism of the renormalized Hamiltonian obtained by Gutzwiller projection of holes on one sublattice and doublons on another sublattice, further implemented by the Gutzwiller approximation, is illuminating enough to give insight into this exotic physics.

IV. STRONGLY CORRELATED BINARY ALLOYS

In this section we will discuss the physics of hole projection in the context of the strongly correlated limit of binary alloys, modeled with the Hubbard model in the presence of a binary disorder. The Hamiltonian for this system is

$$\mathcal{H} = -t \sum_{\langle ij \rangle} c^{\dagger}_{i\sigma} c_{j\sigma} + U \sum_i n_{i\uparrow} n_{i\downarrow} - \sum_i (\mu - \epsilon_i) n_i, \quad (26)$$

where ϵ_i is the random on-site energy drawn from the probability distribution function

$$p_{\epsilon}(\epsilon_i) = x\delta\left(\epsilon_i + \frac{V}{2}\right) + (1-x)\delta\left(\epsilon_i - \frac{V}{2}\right). \quad (27)$$

Here, x and $1-x$ are the fractions of the lattice sites with energies $-\frac{V}{2}$ and $\frac{V}{2}$, respectively. We label sites with $\epsilon(i) = -V/2$ as A sites and sites with $\epsilon(i) = V/2$ as B sites. At half filling, the above Hamiltonian is particle-hole symmetric only if the percentages of A and B sites are equal.

Most of the earlier studies have solved this model using variants of DMFT in the weak to intermediate limit of U/t [27–30]. Using DMFT+QMC, this model has also been solved at finite temperature in the limit of sufficiently large U and V [29]. We are interested in the strongly correlated, strongly disordered limit of this model, that is, $U \sim V \gg t$. The single-site energetics is similar to IHM; that is, holes are projected out from Hilbert space at A sites and doublons are projected out from Hilbert space at B sites. The difference here is that the hole-projected sites and doublon-projected sites are randomly distributed on the lattice in each disorder configuration. This makes all three types of nearest neighbor bonds possible: AA, BB, and AB. Also in three-site processes, as we will show later, there are many more hopping processes possible which do not occur for IHM. Every disorder configuration has a different combination of two-site and three-site hopping terms due to different environment of a site in each configuration.

A. Similarity transformation

The nearest neighbor hopping processes between two sites can be classified as follows depending upon which sites are involved in the hopping—AA sites, BB sites, or AB sites—and whether the hopping process changes the number of doublons or not:

$$\begin{aligned} H_t^{AA} &= H_t^{+}{}_{A\to A} + H_t^{-}{}_{A\to A} + H_t^{0}{}_{A\to A}, \\ H_t^{BB} &= H_t^{+}{}_{B\to B} + H_t^{-}{}_{B\to B} + H_t^{0}{}_{B\to B}, \\ H_t^{AB} &= H_t^{+}{}_{A\to B} + H_t^{+}{}_{B\to A} + H_t^{-}{}_{A\to B} + H_t^{-}{}_{B\to A} \\ &\quad + H_t^{0}{}_{A\to B} + H_t^{0}{}_{B\to A}. \end{aligned} \quad (28)$$

Since an A-type site has doublons allowed in the low-energy sectors and holes should be projected out while on B-type sites the reverse happens, one needs to do different similarity transformations on the local Hamiltonian depending on whether the bond is AA type, BB type, or AB type:

$$\begin{aligned} iS^{AA} &= \frac{1}{U}(H_t^{+}{}_{A\to A} - H_t^{-}{}_{A\to A}), \\ iS^{BB} &= \frac{1}{U}(H_t^{+}{}_{B\to B} - H_t^{-}{}_{B\to B}), \\ iS^{AB} &= \frac{1}{U+V}(H_t^{+}{}_{A\to B} - H_t^{-}{}_{B\to A}) \\ &\quad + \frac{1}{V}\left(H_t^{0}{}_{A\to B} - H_t^{0}{}_{B\to A}\right). \end{aligned} \quad (29)$$

Note that S^{AA} and S^{BB} are perturbative in t/U while S^{AB} has terms which are perturbative in $t/(U+V)$ or t/V.

If we consider the commutators of the type $[S^{\alpha\beta}, H_t^{\alpha\beta}]$ and $[S^{\alpha\beta}, [S^{\alpha\beta}, H_0^{\alpha\beta}]]$, we get terms connecting the low-energy sector to the high-energy sector which must be removed through suitable similarity transformation. The terms that do not interconnect the low-energy sector and the high-energy sector constitute the effective Hamiltonian. The effective Hamiltonian itself is a function of disorder configuration. In a disorder configuration, dimer terms in $H_{\rm eff}$ depend on whether bonds are AA, BB, or AB type:

$$\begin{aligned}\mathcal{H}_{\rm eff} &= H_0 + {H_t^0}_{A\to A} + {H_t^0}_{B\to B} + {H_t^+}_{B\to A} + {H_t^-}_{A\to B} \\ &+ \frac{1}{U}[{H_t^+}_{A\to A}, {H_t^-}_{A\to A}] + \frac{1}{U}[{H_t^+}_{B\to B}, {H_t^-}_{B\to B}] \\ &+ \frac{1}{U+V}[{H_t^+}_{A\to B}, {H_t^-}_{B\to A}] + \frac{1}{V}\left[{H_t^0}_{A\to B}, {H_t^0}_{B\to A}\right] \\ &+ \frac{1}{2}\left(\frac{1}{U}+\frac{1}{V}\right)\left[{H_t^+}_{A\to A} + {H_t^-}_{B\to B}, {H_t^0}_{B\to A}\right] \\ &- \frac{1}{2}\left(\frac{1}{U}+\frac{1}{V}\right)\left[{H_t^-}_{A\to A} + {H_t^-}_{B\to B}, {H_t^0}_{A\to B}\right].\end{aligned} \tag{30}$$

B. Effective low-energy Hamiltonian in terms of projected fermions

Now we represent the effective low-energy Hamiltonian of Eq. (30) in terms of projected fermionic operators on A and B sites as defined in Eqs. (12) and (13). Let us first consider the $O(t)$ hopping terms which are confined in the low-energy Hilbert space and are represented as

$$\begin{aligned}H_{1,\rm low}^{A_i,A_j} &= H_{tA\to A}^0(i,j) = -t\sum_\sigma[\tilde{c}_{iA\sigma}^\dagger \tilde{c}_{jA\sigma} + \text{H.c.}], \\ H_{1,\rm low}^{B_i,B_j} &= H_{tB\to B}^0(i,j) = -t\sum_\sigma[\tilde{\tilde{c}}_{iB\sigma}^\dagger \tilde{\tilde{c}}_{jB\sigma} + \text{H.c.}].\end{aligned} \tag{31}$$

Here, ${H_t^0}_{A\to A}$ involves hopping of a doublon while ${H_t^0}_{B\to B}$ involves hopping of a hole:

$$\begin{aligned}H_{1,\rm low}^{A_i,B_j} &= H_{tA\to B}^-(i,j) + H_{tB\to A}^+(i,j) \\ &= -t\sum_\sigma[\tilde{c}_{iA\sigma}^\dagger \tilde{\tilde{c}}_{jB\sigma} + \text{H.c.}].\end{aligned} \tag{32}$$

$O(t^2/U)$ dimer terms. Now we consider $O(t^2/U)$ dimer terms obtained from $\frac{1}{U}[{H_t^+}_{\alpha\to\alpha}, {H_t^-}_{\alpha\to\alpha}]$ terms with $\alpha = A, B$. Let us first look at the AA term. $\frac{1}{U}[{H_t^+}_{A\to A}, {H_t^-}_{A\to A}] \sim -\frac{1}{U}{H_t^-}_{A\to A}{H_t^+}_{A\to A}$ since the first term in the commutator requires a hole to start with which lies in the high-energy sector for A-type sites. The dimer term corresponding to this commutator is

$$\begin{aligned}H_{\rm dimer}^{A_i,A_j} = -\frac{t^2}{U}\sum_\sigma\big[&{X_{iA}}^{\sigma\leftarrow\sigma}{X_{jA}}^{\bar\sigma\leftarrow\bar\sigma} \\ &- {X_{iA}}^{\sigma\leftarrow\bar\sigma}{X_{jA}}^{\bar\sigma\leftarrow\sigma} + j\leftrightarrow i\big].\end{aligned} \tag{33}$$

This in terms of projected operators can be expressed as

$$\begin{aligned}&\frac{J}{2}\sum_\sigma[\tilde{c}_{iA\bar\sigma}\tilde{c}_{iA\sigma}^\dagger\tilde{c}_{jA\sigma}\tilde{c}_{jA\bar\sigma}^\dagger - \tilde{c}_{iA\bar\sigma}\tilde{c}_{iA\bar\sigma}^\dagger\tilde{c}_{jA\sigma}\tilde{c}_{jA\sigma}^\dagger] \\ &= J\mathcal{P}_h\left(S_{iA}\cdot S_{jA} - \frac{(2-n_{iA})(2-n_{jA})}{4}\right)\mathcal{P}_h\end{aligned} \tag{34}$$

with $J = 4t^2/U$. A factor of $4 = 2\times 2$ comes from spin summation and from hoppings from i to j site first or vice versa. A similar analysis can be extended in the case of B sites. $\frac{1}{U}[{H_t^+}_{B\to B}, {H_t^-}_{B\to B}] \sim -\frac{1}{U}{H_t^-}_{B\to B}{H_t^+}_{B\to B}$ since the first term in the commutator requires a doublon to start with which lies in the high-energy sector for B-type sites. The dimer term corresponding to this commutator is

$$\begin{aligned}H_{\rm dimer}^{B_i,B_j} = -\frac{t^2}{U}\sum_{\langle ij\rangle,\sigma}\big[&{X_{iB}}^{\sigma\leftarrow\sigma}{X_{jB}}^{\bar\sigma\leftarrow\bar\sigma} \\ &- {X_{iB}}^{\sigma\leftarrow\bar\sigma}{X_{jB}}^{\bar\sigma\leftarrow\sigma} + j\leftrightarrow i\big].\end{aligned} \tag{35}$$

Again, in terms of projected operators it is

$$\begin{aligned}&-\frac{J}{2}\sum_\sigma[\tilde{\tilde{c}}_{iB\sigma}^\dagger\tilde{\tilde{c}}_{iB\sigma}\tilde{\tilde{c}}_{jB\bar\sigma}^\dagger\tilde{\tilde{c}}_{jB\bar\sigma} - \tilde{\tilde{c}}_{iB\sigma}^\dagger\tilde{\tilde{c}}_{iB\bar\sigma}\tilde{\tilde{c}}_{jB\bar\sigma}^\dagger\tilde{\tilde{c}}_{jB\sigma}] \\ &= J\mathcal{P}_d\left(S_{iB}\cdot S_{jB} - \frac{n_{iB}n_{jB}}{4}\right)\mathcal{P}_d.\end{aligned} \tag{36}$$

There are also $t^2/(U+V)$ order terms obtained from hopping of a spin-1/2 from site A to B and back. In $H_{\rm eff}$ the corresponding term for this process is $\frac{1}{U+V}[{H_t^+}_{A\to B}, {H_t^-}_{B\to A}]$ which, as explained in the section on IHM, can be expressed as

$$H_{\rm dimer}^{A_i,B_j} = J_1[S_{iA}\cdot S_{jB} - (2-\hat{n}_{iA})\hat{n}_{jB}/4] \tag{37}$$

with $J_2 = \frac{2t^2}{U+V}$. Note that all the above expressions are defined in projected Hilbert space.

The dimer term corresponding to $[{H_t^0}_{A\to B}, {H_t^0}_{B\to A}]$ involves hopping of a particle or a doublon from one site to the nearest neighbor site and back to the initial site as shown in Fig. 5. This process is of order t^2/V and the corresponding expression is given in Eq. (16).

$O(t^2/U)$ trimer terms. Since on each site there is possibility of having an A-type site or B-type site, in total there are 8 trimer terms possible arising from various commutators in $H_{\rm eff}$. Trimer terms from the commutator involving only A-type sites $\frac{1}{U}[{H_t^+}_{A\to A}, {H_t^-}_{A\to A}]$ involve hopping of a particle from the intermediate site resulting in the formation of a doublon in the nearest neighbor site and the other doublon unpairs in two ways: one in the spin-preserving way, the other in the spin-flip way, as shown in Fig. 16. Eventually we get $H_{\rm trimer}^{AAA}(i,j,k)$ as

$$\begin{aligned}&-\frac{t^2}{U}\sum_\sigma\left[{X_{jA}}^{\sigma\leftarrow 0}{X_{kA}}^{\bar\sigma\leftarrow d}{X_{iA}}^{d\leftarrow\bar\sigma}{X_{jA}}^{0\leftarrow\sigma} + \text{H.c.}\right] \\ &+\frac{t^2}{U}\sum_\sigma\left[{X_{jA}}^{\sigma\leftarrow 0}{X_{kA}}^{\bar\sigma\leftarrow d}{X_{iA}}^{d\leftarrow\sigma}{X_{jA}}^{0\leftarrow\bar\sigma} + \text{H.c.}\right] \\ &= \frac{t^2}{U}\sum_\sigma[\tilde{c}_{iA\sigma}^\dagger\tilde{c}_{jA\bar\sigma}\tilde{c}_{jA\bar\sigma}^\dagger\tilde{c}_{kA\sigma} - \tilde{c}_{iA\bar\sigma}^\dagger\tilde{c}_{jA\sigma}\tilde{c}_{jA\sigma}^\dagger\tilde{c}_{kA\sigma}] + \text{H.c.}\end{aligned}$$

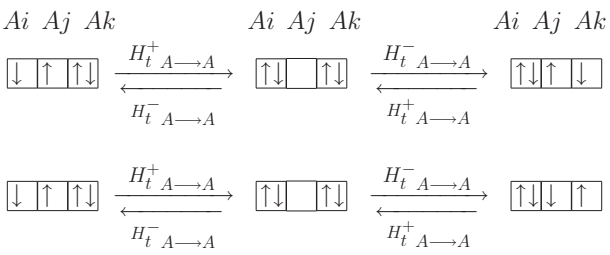

FIG. 16. Trimer term on AAA sites for correlated binary alloy model.

$$= \frac{t^2}{U}\sum_\sigma \mathcal{P}_h[c^\dagger_{iA\sigma}(1-\hat{n}_{jA\bar{\sigma}})c_{kA\sigma} + c^\dagger_{iA\bar{\sigma}}c^\dagger_{jA\sigma}c_{jA\bar{\sigma}}c_{kA\sigma} + \text{H.c.}]\mathcal{P}_h. \tag{38}$$

A similar trimer term on BBB sites is obtained from $\frac{1}{U}[H_t^+{}_{B\to B}, H_t^-{}_{B\to B}]$. In the BBB trimer terms, the effective next nearest neighbor hopping of hole takes place, just as in AAA terms it is the effective next nearest neighbor hopping of a doublon which takes place. The corresponding trimer term can be expressed as

$$\begin{aligned} H^{BBB}_{\text{trimer}} &= -\frac{t^2}{U}\sum_\sigma \left[X^{\sigma\leftarrow 0}_{iB}X^{\bar{\sigma}\leftarrow d}_{jB}X^{d\leftarrow\bar{\sigma}}_{jB}X^{0\leftarrow\sigma}_{kB} + \text{H.c.}\right] \\ &\quad + \frac{t^2}{U}\sum_\sigma \left[X^{\bar{\sigma}\leftarrow 0}_{iB}X^{\sigma\leftarrow d}_{jB}X^{d\leftarrow\bar{\sigma}}_{jB}X^{0\leftarrow\sigma}_{kB} + \text{H.c.}\right] \\ &= -\frac{t^2}{U}\sum_\sigma [\tilde{\tilde{c}}^\dagger_{iB\sigma}\tilde{\tilde{c}}^\dagger_{jB\bar{\sigma}}\tilde{\tilde{c}}_{jB\bar{\sigma}}\tilde{\tilde{c}}_{kB\sigma} - \tilde{\tilde{c}}^\dagger_{iB\bar{\sigma}}\tilde{\tilde{c}}^\dagger_{jB\sigma}\tilde{\tilde{c}}_{jB\bar{\sigma}}\tilde{\tilde{c}}_{kB\sigma}] \\ &= -\frac{t^2}{U}\sum_\sigma \mathcal{P}_d(c^\dagger_{iB\sigma}n_{jB\bar{\sigma}}c_{kB\sigma} - c^\dagger_{iB\bar{\sigma}}c^\dagger_{jB\sigma}c_{jB\bar{\sigma}}c_{kB\sigma} \\ &\quad + \text{H.c.})\mathcal{P}_d. \end{aligned} \tag{39}$$

Then there are ABA- and BAB-type trimer terms, which are of order t^2/V. Note that similar terms also appeared in IHM and are represented in Fig. 6 and Fig. 7. Below we summarize their forms for the case of the binary alloy model:

$$H^{Ai,Bj,Ak}_{\text{trimer}} = -\frac{t^2}{V}\sum_\sigma \mathcal{P}(c^\dagger_{kA\sigma}[n_{jB\bar{\sigma}}c_{iA\sigma} - c_{iA\bar{\sigma}}c^\dagger_{jB\bar{\sigma}}c_{jB\sigma}])\mathcal{P}, \tag{40}$$

$$H^{Bi,Aj,Bk}_{\text{trimer}} = -\frac{t^2}{V}\sum_\sigma \mathcal{P}\{c_{kB\sigma}[(1-n_{iA\bar{\sigma}})c^\dagger_{jB\sigma} + c^\dagger_{iA\sigma}c_{iA\bar{\sigma}}c^\dagger_{jB\bar{\sigma}}]\}\mathcal{P}. \tag{41}$$

AAB and BBA trimer terms. Next we consider the remaining trimer terms, namely, AAB (or BAA) and BBA (or ABB) type terms. We would like to emphasize that these terms never appear in strongly correlated limit of IHM presented in earlier section and are characteristic of random arrangement of A- and B-type sites in the binary alloy model.

The AAB trimer terms, shown in Fig. 17, arise from the commutator $\frac{t^2(U+V)}{2UV}[H_t^+{}_{A\to A}, H_t^0{}_{B\to A}] \sim -\frac{K}{t^2}H_t^0{}_{B\to A}H_t^+{}_{A\to A}$ where we have defined the coupling strength for this term $K = \frac{t^2(U+V)}{2UV}$. This is because the first term of the commutator requires a hole at the intermediate A site to begin with which is energetically unfavorable. As shown in Fig. 17, this consists of the usual spin-preserving and spin-flip terms. In one case, the spin at the intermediate site remains the same as the initial state and in the other case it flips.

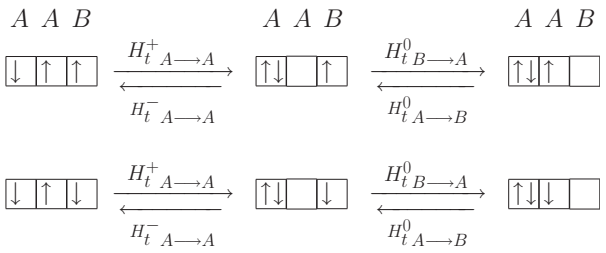

FIG. 17. AAB trimer processes for correlated binary alloy model.

The fermionic representation of $H^{A_i,A_k,B_j}_{\text{trimer}}$ is as follows:

$$\begin{aligned} &-K\sum_\sigma \eta(\sigma)\left[X^{\sigma\leftarrow 0}_{kA}X^{0\leftarrow\sigma}_{jB}X^{d\leftarrow\bar{\sigma}}_{iA}X^{0\leftarrow\sigma}_{kA}\right. \\ &\left. + X^{\bar{\sigma}\leftarrow 0}_{kA}X^{0\leftarrow\bar{\sigma}}_{jB}X^{d\leftarrow\bar{\sigma}}_{iA}X^{0\leftarrow\sigma}_{kA}\right] \\ &= K\sum_\sigma(\tilde{c}^\dagger_{iA\sigma}\tilde{c}_{kA\bar{\sigma}}\tilde{c}^\dagger_{kA\bar{\sigma}}\tilde{\tilde{c}}_{jB\sigma} - \tilde{c}^\dagger_{iA\sigma}\tilde{c}_{kA\sigma}\tilde{c}^\dagger_{kA\bar{\sigma}}\tilde{\tilde{c}}_{jB\bar{\sigma}}) \\ &= K\sum_\sigma \mathcal{P}[c^\dagger_{iA\sigma}(1-n_{kA\bar{\sigma}})c_{jB\sigma} + c^\dagger_{iA\sigma}c^\dagger_{kA\bar{\sigma}}c_{kA\sigma}c_{jB\bar{\sigma}}]\mathcal{P}. \end{aligned} \tag{42}$$

Similarly, the BBA trimer terms appear from the commutator $K[H_t^+{}_{B\to B}, H_t^0{}_{B\to A}] \sim -\frac{K}{t^2}H_t^0{}_{B\to A}H_t^+{}_{B\to B}$. The first term in the commutator requires a doublon at the intermediate site B to start with which is energetically unfavorable. As shown in Fig. 18, these terms also come in two variants, spin preserving and spin flip at the intermediate site.

Below we represent $H^{B_j,B_l,A_i}_{\text{trimer}}$ in terms of X operators and then in terms of projected operators as

$$\begin{aligned} &-K\sum_\sigma \eta(\sigma)\left[X^{d\leftarrow\bar{\sigma}}_{iA}X^{\bar{\sigma}\leftarrow d}_{lB}X^{d\leftarrow\bar{\sigma}}_{lB}X^{0\leftarrow\sigma}_{jB}\right. \\ &\left. + X^{d\leftarrow\sigma}_{iA}X^{\sigma\leftarrow d}_{lB}X^{d\leftarrow\bar{\sigma}}_{lB}X^{0\leftarrow\sigma}_{jB}\right] \end{aligned}$$

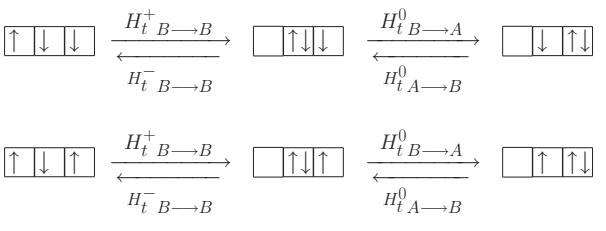

FIG. 18. BBA trimer processes for correlated binary alloy model.

$$= -K \sum_{\sigma} (\tilde{c}^{\dagger}_{iA\sigma} \tilde{\tilde{c}}^{\dagger}_{lB\bar{\sigma}} \tilde{\tilde{c}}_{lB\bar{\sigma}} \tilde{\tilde{c}}_{jB\sigma} - \tilde{c}^{\dagger}_{iA\sigma} \tilde{\tilde{c}}^{\dagger}_{lB\bar{\sigma}} \tilde{\tilde{c}}_{lB\sigma} \tilde{\tilde{c}}_{jB\bar{\sigma}})$$

$$= -K \sum_{\sigma} \mathcal{P}(c^{\dagger}_{iA\sigma} n_{lB\bar{\sigma}} c_{jB\sigma} - c^{\dagger}_{iA\sigma} c^{\dagger}_{lB\bar{\sigma}} c_{lB\sigma} c_{jB\bar{\sigma}})\mathcal{P}. \quad (43)$$

The terms from the commutators $[H^{-}_{t\ A\to A}, H^{0}_{t\ A\to B}]$ and $[H^{-}_{t\ B\to B}, H^{0}_{t\ A\to B}]$ are the Hermitian conjugate terms of the trimer terms in Eqs. (42) and (43) and are represented by the lower arrows in Figs. 17 and 18.

C. Gutzwiller approximation

After finding various terms in the low-energy effective Hamiltonian for the strongly correlated binary disorder model, we will now evaluate Gutzwiller factors for various terms in $H_{\rm eff}$ of Eq. (30). The low-energy effective Hamiltonian for binary alloys consists of certain dimer and trimer terms and for some of these terms we have already found the Gutzwiller factors in the section on IHM. However here, unlike in IHM, the densities on A or B sites are not homogeneous. They are site dependent and depend on the local environment. Let us first consider the hopping process of $O(t)$ between two neighboring sites. Within the Gutzwiller approximation

$$\begin{aligned} H^{A_i,A_j}_{1,\rm low} &= -t \sum_{\sigma} \mathcal{P}_h [c^{\dagger}_{iA\sigma} c_{jA\sigma} + \text{H.c.}]\mathcal{P}_h \\ &= -t \sum_{\sigma} g^{AA}_{t\sigma}(i,j)[c^{\dagger}_{iA\sigma} c_{jA\sigma} + \text{H.c.}], \\ H^{B_i,B_j}_{1,\rm low} &= -t \sum_{\sigma} \mathcal{P}_d [c^{\dagger}_{iB\sigma} c_{jB\sigma} + \text{H.c.}]\mathcal{P}_d \\ &= -t \sum_{\sigma} g^{BB}_{t\sigma}(i,j)[c^{\dagger}_{iB\sigma} c_{jB\sigma} + \text{H.c.}], \\ H^{A_i,B_j}_{1,\rm low} &= -t \sum_{\sigma} \mathcal{P} [c^{\dagger}_{iA\sigma} c_{jB\sigma} + \text{H.c.}]\mathcal{P} \\ &= -t \sum_{\sigma} g^{AB}_{t\sigma}(i,j)[c^{\dagger}_{iA\sigma} c_{jB\sigma} + \text{H.c.}]. \end{aligned} \quad (44)$$

As explained for AB terms in the section on IHM, one can evaluate these Gutzwiller factors by evaluating probability for hopping process on corresponding bonds within the projected and unprojected Hilbert space. By doing an exercise similar to the one explained in the section on IHM, we obtain

$$\begin{aligned} g^{AA}_{t\sigma}(i,j) &= \sqrt{\frac{(\mathbf{n}_{iA}-1)(\mathbf{n}_{jA}-1)}{\mathbf{n}_{iA\sigma}\mathbf{n}_{jA\sigma}}}, \\ g^{BB}_{t\sigma}(i,j) &= \sqrt{\frac{(1-\mathbf{n}_{iB})(1-\mathbf{n}_{jB})}{(1-\mathbf{n}_{iB\sigma})(1-\mathbf{n}_{jB\sigma})}}, \\ g^{AB}_{t\sigma}(i,j) &= \sqrt{\frac{(\mathbf{n}_{iA}-1)(1-\mathbf{n}_{jB})}{\mathbf{n}_{iA\sigma}(1-\mathbf{n}_{jB\sigma})}}. \end{aligned} \quad (45)$$

Next let us consider the renormalization of $O(t^2/U)$ dimer terms which are also of three types depending upon the bond under consideration in a given disorder configuration. Within the Gutzwiller approximation, couplings in Eqs. (34), (36), and (37) get rescaled with the corresponding Gutzwiller factors to give

$$\begin{aligned} H^{A_i,A_j}_{\rm dimer} &= J g^{AA}_{s}(i,j)\left(S_{iA}\cdot S_{jA} - \frac{(2-n_{iA})(2-n_{jA})}{4}\right), \\ H^{B_i,B_j}_{\rm dimer} &= J g^{BB}_{s}(i,j)\left(S_{iB}\cdot S_{jB} - \frac{n_{iB}n_{jB}}{4}\right), \\ H^{A_i,B_j}_{\rm dimer} &= J_2 g^{AB}_{s}(i,j)\left(S_{iA}\cdot S_{jB} - \frac{(2-n_{iA})n_{jB}}{4}\right). \end{aligned} \quad (46)$$

The corresponding Gutzwiller factors are obtained, as explained for an AB term in the section on IHM, to be

$$\begin{aligned} g^{AA}_{s}(i,j) &= \frac{1}{\sqrt{\mathbf{n}_{iA\uparrow}\mathbf{n}_{iA\downarrow}\mathbf{n}_{jA\uparrow}\mathbf{n}_{jA\downarrow}}}, \\ g^{BB}_{s}(i,j) &= \frac{1}{\sqrt{(1-\mathbf{n}_{iB\uparrow})(1-\mathbf{n}_{iB\downarrow})(1-\mathbf{n}_{jB\uparrow})(1-\mathbf{n}_{jB\downarrow})}}, \\ g^{AB}_{s}(i,j) &= \frac{1}{\sqrt{\mathbf{n}_{iA\uparrow}\mathbf{n}_{iA\downarrow}(1-\mathbf{n}_{jB\uparrow})(1-\mathbf{n}_{jB\downarrow})}}. \end{aligned} \quad (47)$$

In the calculation of Gutzwiller factors for the trimer terms, the intermediate step is unimportant; only the initial and final states are used to calculate the probabilities. The renormalized form of the AAA trimer term which is written in Eq. (38) is given below:

$$\begin{aligned} H^{A_i,A_j,A_k}_{\rm trimer} = \frac{t^2}{U}\sum_{\sigma}\big[& g^{AAA}_{1\sigma}(i,j,k) c^{\dagger}_{iA\sigma}(1-\hat{n}_{jA\bar{\sigma}}) c_{kA\sigma} \\ & + g^{AAA}_{2\sigma}(i,j,k) c^{\dagger}_{iA\bar{\sigma}} c^{\dagger}_{jA\sigma} c_{jA\bar{\sigma}} c_{kA\sigma} + \text{H.c.}\big]. \end{aligned} \quad (48)$$

The processes in projected and unprojected spaces for the calculation of $g_{1\uparrow}$ are shown in Fig. 19. The probability of the process in the unprojected basis is $(1-\mathbf{n}_{iA\uparrow})\mathbf{n}_{iA\uparrow}(1-\mathbf{n}_{jA\downarrow})^2\mathbf{n}_{kA\uparrow}(1-\mathbf{n}_{kA\uparrow})$ and in the projected basis it is $(\mathbf{n}_{iA}-1)(1-\mathbf{n}_{iA\uparrow})(1-\mathbf{n}_{jA\downarrow})^2(\mathbf{n}_{kA}-1)(1-\mathbf{n}_{kA\uparrow})$. The Gutzwiller factor then comes out to be

$$g^{AAA}_{1\uparrow}(i,j,k) = \sqrt{\frac{(\mathbf{n}_{iA}-1)(\mathbf{n}_{kA}-1)}{\mathbf{n}_{iA\uparrow}\mathbf{n}_{kA\uparrow}}}. \quad (49)$$

In Fig. 19(b), the processes in unprojected and projected spaces required for the calculation of $g_{2\sigma}$ are shown for which the total probability in the unprojected basis is $(1-\mathbf{n}_{iA\downarrow})\mathbf{n}_{jA\downarrow}(1-\mathbf{n}_{jA\uparrow})\mathbf{n}_{kA\uparrow}(1-\mathbf{n}_{kA\uparrow})\mathbf{n}_{jA\uparrow}(1-\mathbf{n}_{jA\downarrow})\mathbf{n}_{iA\downarrow}$ and in the projected basis is $(1-\mathbf{n}_{iA\downarrow})(1-\mathbf{n}_{jA\uparrow})(\mathbf{n}_{kA}-1)(1-\mathbf{n}_{kA\uparrow})(1-\mathbf{n}_{jA\downarrow})(\mathbf{n}_{iA}-1)$. The Gutzwiller factor then comes out to be

$$g^{AAA}_{2\sigma}(i,j,k) = \sqrt{\frac{(\mathbf{n}_{kA}-1)(\mathbf{n}_{iA}-1)}{\mathbf{n}_{jA\uparrow}\mathbf{n}_{jA\downarrow}\mathbf{n}_{kA\sigma}\mathbf{n}_{iA\bar{\sigma}}}}. \quad (50)$$

Similarly, the BBB trimer terms of Eq. (39) can be obtained by replacing $\mathbf{n}_{A\sigma}$ with $(1-\mathbf{n}_{B\sigma})$ and $(\mathbf{n}_A-1)$ with $(1-\mathbf{n}_B)$ in the above two equations.

Now we consider the trimer terms of ABA and BAB types for which we also calculated the Gutzwiller factors in the section on IHM. The renormalized form of these terms under

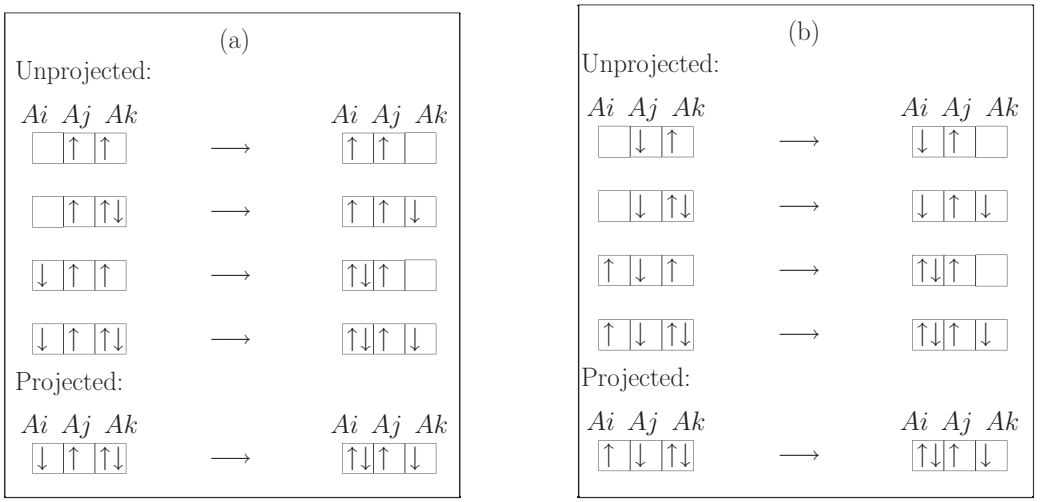

FIG. 19. (a) Processes involved in the calculation of $g_{1\sigma}$ and $g_{2\sigma}$ which are renormalization Gutzwiller factors for *AAA* trimer terms.

the Gutzwiller approximation is

$$H_{\text{trimer}}^{Ai,Bj,Ak} = -\frac{t^2}{V}\sum_{\sigma} c_{kA\sigma}^{\dagger}\left[g_{1\sigma}^{ABA}(i,j,k)n_{jB\bar{\sigma}}c_{iA\sigma} - g_{2\sigma}^{ABA}(i,j,k)c_{iA\bar{\sigma}}c_{jB\bar{\sigma}}^{\dagger}c_{jB\sigma}\right], \tag{51}$$

$$H_{\text{trimer}}^{Bj,Ai,Bl} = -\frac{t^2}{V}\sum_{\sigma} c_{lB\sigma}\left[g_{1\sigma}^{BAB}(j,i,l)(1-n_{iA\bar{\sigma}})c_{jB\sigma}^{\dagger} + g_{2\sigma}^{BAB}(j,i,l)c_{iA\sigma}^{\dagger}c_{iA\bar{\sigma}}c_{jB\bar{\sigma}}^{\dagger}\right]. \tag{52}$$

Now we will calculate Gutzwiller factors for these trimer terms shown in Fig. 6 and Fig. 7. Figure 6(a) shows hopping of an $\uparrow$ electron from an A site to its next nearest neighbor A sites with a spin $\downarrow$ on the intermediate B site being preserved. In the unprojected basis, the probability for this process to happen is $\mathbf{n}_{iA\uparrow}\mathbf{n}_{jB\downarrow}^2(1-\mathbf{n}_{kA\uparrow})(1-\mathbf{n}_{iA\uparrow})\mathbf{n}_{kA\uparrow}$. It is to be noted that processes with either a down-type particle or a doublon at the intermediate B site have been considered in the unprojected space. Likewise, the probability for the process to happen in the projected basis is $(\mathbf{n}_{iA}-1)(1-\mathbf{n}_{kA\uparrow})\mathbf{n}_{B\downarrow}^2(\mathbf{n}_{kA}-1)(1-\mathbf{n}_{iA\uparrow})$. Therefore, the Gutzwiller factor for this process is

$$g_{1\uparrow}^{ABA}(i,j,k) = \sqrt{\frac{(\mathbf{n}_{iA}-1)(\mathbf{n}_{kA}-1)}{\mathbf{n}_{iA\uparrow}\mathbf{n}_{kA\uparrow}}}. \tag{53}$$

Figure 6(b) depicts hopping processes on the A sublattice in which spin on the intermediate B site gets flipped. The probability in the unprojected basis for this process to occur is $\mathbf{n}_{iA\downarrow}\mathbf{n}_{jB\uparrow}(1-\mathbf{n}_{jB\downarrow})(1-\mathbf{n}_{kA\uparrow})(1-\mathbf{n}_{iA\downarrow})\mathbf{n}_{jB\downarrow}(1-\mathbf{n}_{jB\uparrow})\mathbf{n}_{kA\uparrow}$, whereas that in the projected basis is $(\mathbf{n}_{iA}-1)\mathbf{n}_{jB\uparrow}(1-\mathbf{n}_{kA\uparrow})(1-\mathbf{n}_{iA\downarrow})\mathbf{n}_{jB\downarrow}(\mathbf{n}_{kA}-1)$ resulting in the Gutzwiller factor

$$g_{2\sigma}^{ABA}(i,j,k) = \sqrt{\frac{(\mathbf{n}_{iA}-1)(\mathbf{n}_{kA}-1)}{\mathbf{n}_{iA\bar{\sigma}}\mathbf{n}_{kA\sigma}(1-\mathbf{n}_{jB\uparrow})(1-\mathbf{n}_{jB\downarrow})}}. \tag{54}$$

Similarly, we can obtain the Gutzwiller factors $g_{1\sigma}^{BAB}(i,j,l)$ and $g_{2\sigma}^{BAB}(i,j,l)$ from the above two equations by replacing $\mathbf{n}_{A\sigma}$ with $(1-\mathbf{n}_{B\sigma})$ and $(\mathbf{n}_A-1)$ with $(1-\mathbf{n}_B)$.

Now we will focus on the Gutzwiller factors of the new trimer terms which arise out of the *AAB* and *BBA* processes. The renormalized AAB and BBA trimer terms can be expressed as

$$H_{\text{trimer}}^{A_i,A_k,B_j} = K\sum_{\sigma}\left[g_{1\sigma}^{AAB}(i,k,j)c_{iA\sigma}^{\dagger}(1-n_{kA\bar{\sigma}})c_{jB\sigma} + g_{2\sigma}^{AAB}(i,k,j)c_{iA\sigma}^{\dagger}c_{kA\bar{\sigma}}^{\dagger}c_{kA\sigma}c_{jB\bar{\sigma}}\right],$$

$$H_{\text{trimer}}^{B_j,B_l,A_i} = -K\sum_{\sigma}\left[g_{1\sigma}^{BBA}(j,l,i)c_{iA\sigma}^{\dagger}n_{lB\bar{\sigma}}c_{jB\sigma} - g_{2\sigma}^{BBA}(j,l,i)c_{iA\sigma}^{\dagger}c_{lB\bar{\sigma}}^{\dagger}c_{lB\sigma}c_{jB\bar{\sigma}}\right]. \tag{55}$$

The *AAB* and *BBA* spin-preserving hoppings as depicted in Figs. 20(a) and 21(a) are effective next nearest neighbor hopping processes, the Gutzwiller factors for which are like nearest neighbor *AB* hopping. If we look at Fig. 20(a) for the processes involved in the calculation of the Gutzwiller factor $g_{1\uparrow}^{AAB}$, we see that the probability of the process in the unprojected basis is $(1-\mathbf{n}_{iA\uparrow})\mathbf{n}_{iA\uparrow}(1-\mathbf{n}_{kA\downarrow})^2(1-\mathbf{n}_{jB\uparrow})\mathbf{n}_{jB\uparrow}$ and in the projected basis it is $(1-\mathbf{n}_{iA\uparrow})(\mathbf{n}_{iA}-1)(1-\mathbf{n}_{kA\downarrow})^2\mathbf{n}_{jB\uparrow}(1-\mathbf{n}_{jB})$ resulting in the Gutzwiller factor

$$g_{1\uparrow}^{AAB}(i,k,j) = \sqrt{\frac{(\mathbf{n}_{iA}-1)(1-\mathbf{n}_{jB})}{\mathbf{n}_{iA\uparrow}(1-\mathbf{n}_{jB\uparrow})}}. \tag{56}$$

It is to be remembered that in the unprojected basis, processes with either an up-spin electron or a hole at the intermediate A site have been considered. In Fig. 21(a), processes involved in the calculation of $g_{1\uparrow}^{BBA}$ have been depicted. The probability of the process in the unprojected basis is $(1-\mathbf{n}_{iA\uparrow})\mathbf{n}_{iA\uparrow}\mathbf{n}_{lB\downarrow}^2(1-\mathbf{n}_{jB\uparrow})\mathbf{n}_{jB\uparrow}$ and in the projected basis is $(1-\mathbf{n}_{iA\uparrow})(\mathbf{n}_{iA}-1)\mathbf{n}_{lB\downarrow}^2(1-\mathbf{n}_{jB})n_{jB\uparrow}$. Then, the Gutzwiller factor is

$$g_{1\uparrow}^{BBA}(j,l,i) = \sqrt{\frac{(\mathbf{n}_{iA}-1)(1-\mathbf{n}_{jB})}{\mathbf{n}_{iA\uparrow}(1-\mathbf{n}_{jB\uparrow})}}, \tag{57}$$

which is the same as $g_{1\uparrow}^{AAB}(i,k,j)$.

The Gutzwiller factors for spin-flip terms depicted in Figs. 20(b) and 21(b) can be found out similarly. For $g_{2\uparrow}^{AAB}(i,k,j)$, the probability in the unprojected space is

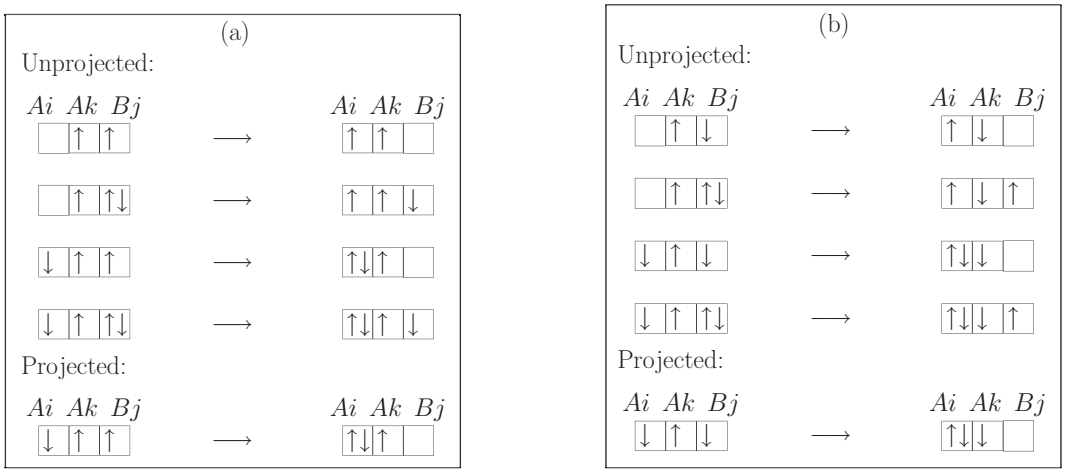

FIG. 20. (a) Processes involved in the calculation of $g_{1\sigma}^{AAB}$. Similar *AAB* physical processes with hole at intermediate *A* site in the unprojected basis are considered in the calculation. (b) Processes involved in calculation of $g_{2\sigma}^{AAB}$.

$(1-\mathbf{n}_{iA\uparrow})\mathbf{n}_{iA\uparrow}(1-\mathbf{n}_{kA\uparrow})(1-\mathbf{n}_{kA\downarrow})\mathbf{n}_{kA\uparrow}\mathbf{n}_{kA\downarrow}\mathbf{n}_{jB\downarrow}(1-\mathbf{n}_{jB\downarrow})$ and in the projected space is $(1-\mathbf{n}_{iA\uparrow})(\mathbf{n}_{iA}-1)(1-\mathbf{n}_{kA\uparrow})(1-\mathbf{n}_{kA\downarrow})\mathbf{n}_{jB\downarrow}(1-\mathbf{n}_{jB})$ resulting in the Gutzwiller factor

$$g_{2\uparrow}^{AAB}(i,k,j)=\sqrt{\frac{(\mathbf{n}_{iA}-1)(1-\mathbf{n}_{jB})}{\mathbf{n}_{kA\uparrow}\mathbf{n}_{kA\downarrow}\mathbf{n}_{iA\uparrow}(1-\mathbf{n}_{jB\downarrow})}}. \quad (58)$$

For $g_{2\uparrow}^{BBA}(j,l,i)$, the probability in the unprojected space is $(1-\mathbf{n}_{iA\uparrow})\mathbf{n}_{iA\uparrow}\mathbf{n}_{lB\uparrow}\mathbf{n}_{lB\downarrow}(1-\mathbf{n}_{lB\uparrow})(1-\mathbf{n}_{lB\downarrow})\mathbf{n}_{jB\downarrow}(1-\mathbf{n}_{jB\downarrow})$ and that in the projected space is $(1-\mathbf{n}_{iA\uparrow})(\mathbf{n}_{iA}-1)\mathbf{n}_{lB\uparrow}\mathbf{n}_{lB\downarrow}\mathbf{n}_{jB\downarrow}(1-\mathbf{n}_{jB})$ leading to the Gutzwiller factor

$$g_{2\uparrow}^{BBA}(j,l,i)=\sqrt{\frac{(\mathbf{n}_{iA}-1)(1-\mathbf{n}_{jB})}{(1-\mathbf{n}_{lB\uparrow})(1-\mathbf{n}_{lB\downarrow})\mathbf{n}_{iA\uparrow}(1-\mathbf{n}_{jB\downarrow})}}. \quad (59)$$

D. Insights into correlated binary alloy from the renormalized Hamiltonian

The renormalized Hamiltonian derived above brings deep insight towards the possible phase diagram of the strongly correlated binary alloy. Let us first focus at the projected hopping terms given in Eq. (44) and the corresponding Gutzwiller factors in Eq. (45). At half filling for $U \gg t$, if the disorder is weak, the system will be an antiferromagnetic Mott insulator because the hopping term is completely projected out. As disorder increases and becomes comparable to U, the local particle density does not remain close to one on all the sites and the Gutzwiller factors $g_{t\sigma}^{\alpha\beta}$ for various hopping processes become finite resulting in finite kinetic energy of the electrons. Also the Mott gap reduces with increase in V. This indicates the possibility of a metallic phase in the system for $V \sim U$. This is consistent with what has been shown within DMFT + coherent potential approximation [35]. In the metallic phase, the quasiparticle weight will be given by the most probable value of the Gutzwiller factors for hopping terms [in Eq. (45)]. Since $V \sim U$, the local electron densities will not deviate much from unity. Hence the Gutzwiller factors $g_{t\sigma}^{\alpha\beta}$ are very small resulting in very small quasiparticle weight in the metallic phase.

Let us now turn our attention to the spin exchange terms in the low-energy Hamiltonian. For the parameter regime

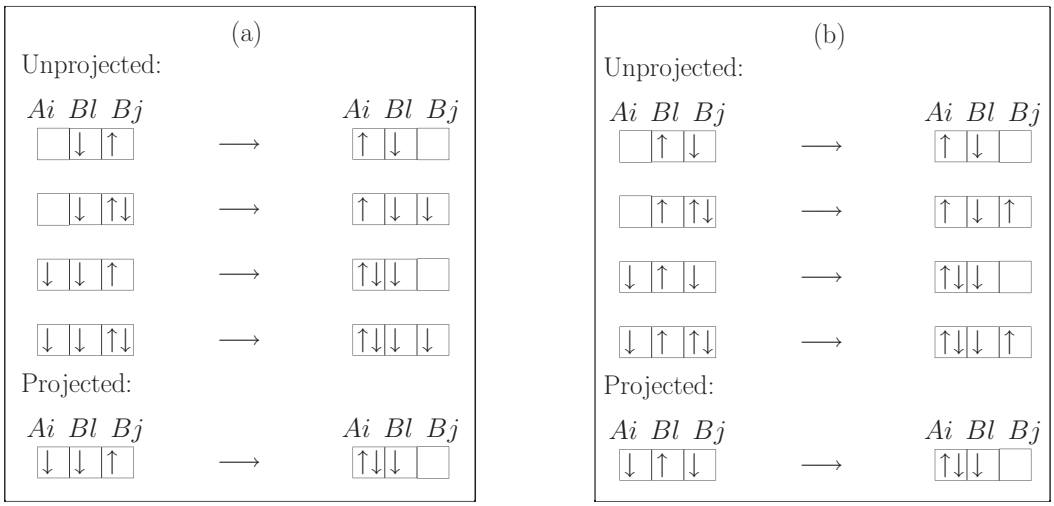

FIG. 21. (a) Processes involved in the calculation of $g_{1\sigma}^{BBA}$. Similar *BBA* physical processes with doublon at intermediate *B* site in the unprojected basis are considered in the calculation. (b) Processes involved in calculation of $g_{2\sigma}^{BBA}$.

$V \sim U \gg t$, since the effective hopping in the projected Hilbert space becomes finite, and the electron density on each site is not one, spin exchange terms might give rise to disordered superconductivity with either d-wave pairing or $d + is$ pairing. Due to the presence of large binary disorder, we might get a disordered superconducting phase coexisting with an incommensurate/discommensurate charge density wave which is a topic of great interest in context of high-T_c superconductors [36].

V. CONCLUSION

In this work, we have extended the idea of Gutzwiller projection for excluding holes from the low-energy Hilbert space, which so far has been developed only for exclusion of doublons, e.g., in context of the hole-doped t-J model. We have discussed variants of the Hubbard model with on-site potentials because of which, in the limit of strong correlations and comparable potential terms, on some sites doublons are projected out from low-energy Hilbert space while from some other sites holes are projected out from the low-energy Hilbert space. In order to understand the physics of these systems, it becomes essential to understand how to carry out Gutzwiller projection for holes. We defined new fermionic operators in the case of hole-projected Hilbert space and derived effective low-energy Hamiltonian for these models by carrying out systematic similarity transformation. We further carried out rescaling of couplings in the effective Hamiltonian using the Gutzwiller approximation to implement the effect of site-dependent projection of holes and doublons. To be specific, we provided details of the similarity transformation and Gutzwiller approximation for the IHM and Hubbard model with binary disorder.

The effective low-energy Hamiltonian derived in both the cases shines light on the possibility of exotic phases. In the half-filled IHM, our renormalized Hamiltonian predicts a half-metal phase followed up by a metal with increase in Δ for $U \sim \Delta$ and a superconducting phase for higher-dimensional ($d \geqslant 2$) systems. Our effective Hamiltonian also explains the nonmonotonic behavior of the Néel temperature as a function of Δ in the AFM phase of the IHM realized for $U \gg t$. In the correlated binary alloy model, for both disorder and e-e interactions being much larger than the hopping amplitude ($V \sim U \gg t$), there is a possible metallic phase which might turn into a very narrow disordered superconducting phase coexisting with a discommensurate charge density wave in two- or higher-dimensional systems with the help of effective next nearest neighbor hopping. The nature of Gutzwiller factors indicates that the metallic phase intervening between the two insulating phases in the IHM or the correlated binary alloy model will be a bad metal with very high effective mass of the quasiparticles.

Although we have considered so far the case of the strongly correlated Hubbard model in the presence of large binary disorder, the formalism can be easily used even in the case of fully random disorder $V(i) \in [-V, V]$. The strongly correlated Hubbard model in the presence of fully random disorder has been mostly studied in the limit of weak disorder mainly in context of high-T_c cuprates [32,37]. The case of strong disorder has been studied in order to understand the effect of impurities like Zn in high-T_c cuprates [38] but that too keeping $V \leqslant U$ so that the constraint of no double occupancy remains intact. But for the limit of strong correlation as well as strong disorder such that $U \sim V \gg t$ the formalism of hole projection is essential and has not been studied before. For $V(i) < 0$ and $|V(i)| > V_c$, where $V_c \gg t$, holes will not be allowed in the low-energy Hilbert space. But due to the limit of strong correlations for the hole-doped case, doublons will not be energetically allowed at other sites of the system which have either $V(i) > 0$ or $V(i) < 0$ but $|V(i)| < V_c$. Hence, even in the case of fully random disorder there will be effectively two type of sites A where holes are projected out from low-energy Hilbert space and B-type sites where doublons are projected out from low-energy Hilbert space, and one can easily use the formalism we have provided for strongly correlated binary alloys. Another situation where this physics is of relevance is a strongly correlated Hubbard model with large attractive impurities randomly distributed over the lattice with $V(i) = -V$ at the impurity sites and $V(i) = 0$ at other sites of the lattice. For $V \sim U \gg t$, at the impurity sites energetics will not allow holes in the low-energy Hilbert space while at all other sites of the lattice for which $V(i) = 0$ large U will not allow for doublons in the low-energy sector for the hole-doped case. Again in this situation one can use the formalism developed here for the case of strongly correlated binary alloys.

To conclude, in this work we have provided an essential tool which has been missing so far in the field of strongly correlated electron systems, that is, the Gutzwiller projection for holes allowing for doublons which happens in many correlated systems in various possible scenarios explained above. We have described its implementation at the level of the Gutzwiller approximation. We would like to mention that so far we have evaluated Gutzwiller factors under the simplest assumption of spin-resolved densities being the same in the projected and unprojected state. In future work we would like to extend this work to find Gutzwiller factors in more general scenarios.

[1] P. Fazekas, *Lecture Notes on Electron Correlation and Magnetism* (World Scientific, Singapore, 1999).

[2] P. W. Anderson, Science **235**, 1196 (1987); S. A. Kivelson, D. S. Rokhsar, and J. P. Sethna, Phys. Rev. B **35**, 8865 (1987); G. Baskaran, Z. Zou, and P. W. Anderson, Solid State Commun. **63**, 973 (1987); G. Kotliar and J. Liu, Phys. Rev. B **38**, 5142 (1988); C. Gros, *ibid.* **38**, 931 (1988); P. W. Anderson, P. A. Lee, M. Randeria, T. M. Rice, N. Trivedi, and F. C. Zhang, J. Phys.: Condens. Matter **16**, R755 (2004); F. C. Zhang and T. M. Rice, Phys. Rev. B **37**, 3759(R) (1988); P. A. Lee, N. Nagaosa, and X. G. Wen, Rev. Mod. Phys. **78**, 17 (2006).

[3] A. L. Fetter and J. D. Walecka, *Quantum Theory of Many-Particle Systems* (Dover Publications, New York, 2003).

[4] B. S. Shastry, Phys. Rev. B **87**, 125124 (2013); Ann. Phys. **343**, 164 (2014).

[5] C. Gros, Ann. Phys. **189**, 53 (1989).

[6] M. C. Gutzwiller, Phys. Rev. **134**, A923 (1964); **137**, A1726 (1965).

[7] T. Ogawa, K. Kanda, and T. Matsubara, Prog. Theor. Phys. **53**, 614 (1975); D. Vollhardt, Rev. Mod. Phys. **56**, 99 (1984); F. C. Zhang, C. Gros, T. M. Rice, and H. Shiba, Supercond. Sci. Technol. **1**, 36 (1988); M. Ogata and A. Himeda, J. Phys. Soc. Jpn. **72**, 374 (2003) ; W. H. Ko, C. P. Nave, and P. A. Lee, Phys. Rev. B **76**, 245113 (2007); B. Edegger, V. N. Muthukumar, and C. Gros, Adv. Phys. **56**, 927 (2007).

[8] M. Fabrizio, A. O. Gogolin, and A. A. Nersesyan, Phys. Rev. Lett. **83**, 2014 (1999); A. P. Kampf, M. Sekania, G. I. Japaridze, and P. Brune, J. Phys.: Condens. Matter **15**, 5895 (2003); S. R. Manmana, V. Meden, R. M. Noack, and K. Schönhammer, Phys. Rev. B **70**, 155115 (2004).

[9] T. Jabben, N. Grewe, and F. B. Anders, Eur. Phys. J. B **44**47 (2005).

[10] A. Garg, H. R. Krishnamurthy, and M. Randeria, Phys. Rev. Lett. **97**, 046403 (2006).

[11] L. Craco, P. Lombardo, R. Hayn, G. I. Japaridze, and E. Muller-Hartmann, Phys. Rev. B **78**, 075121 (2008).

[12] K. Byczuk, M. Sekania, W. Hofstetter, and A. P. Kampf, Phys. Rev. B **79**, 121103 (2009).

[13] A. Garg, H. R. Krishnamurthy, and M. Randeria, Phys. Rev. Lett. **112**, 106406 (2014).

[14] Xin Wang, R. Sensarma, and S. Das Sarma, Phys. Rev. B **89**, 121118(R) (2014).

[15] A. J. Kim, M. Y. Choi, and G. S. Jeon, Phys. Rev. B **89**, 165117 (2014).

[16] S. Bag, A. Garg, and H. R. Krishnamurthy, Phys. Rev. B **91**, 235108 (2015).

[17] N. Paris, K. Bouadim, F. Hebert, G. G. Batrouni, and R. T. Scalettar, Phys. Rev. Lett. **98**, 046403 (2007).

[18] K. Bouadim, N. Paris, F. Hebert, G. G. Batrouni, and R. T. Scalettar, Phys. Rev. B **76**, 085112 (2007).

[19] S. S. Kancharla and E. Dagotto, Phys. Rev. Lett. **98**, 016402 (2007).

[20] A. T. Hoang, J. Phys.: Condens. Matter **22**, 095602 (2010).

[21] M. Messer, R. Desbuquois, T. Uehlinger, G. Jotzu, S. Huber, D. Greif, and T. Esslinger, Phys. Rev. Lett. **115**, 115303 (2015).

[22] A. Samanta and R. Sensarma, Phys. Rev. B **94**, 224517 (2016).

[23] C. Li and Z. Wang, Phys. Rev. B **80**, 125130 (2009).

[24] S. H. Pan *et al.*, Nature (London) **413**, 282 (2001).

[25] H. S. Jarrett *et al.*, Phys. Rev. Lett. **21**, 617 (1968); G. L. Zhao, J. Callaway, and M. Hayashibara, Phys. Rev. B **48**, 15781 (1993); S. K. Kwon, S. J. Youn, and B. I. Min, *ibid.* **62**, 357 (2000); T. Shishidou, A. J. Freeman, and R. Asahi, *ibid.* **64**, 180401(R) (2001).

[26] K. Günter, T. Stöferle, H. Moritz, M. Köhl, and T. Esslinger, Phys. Rev. Lett. **96**, 180402 (2006); S. Ospelkaus, C. Ospelkaus, O. Wille, M. Succo, P. Ernst, K. Sengstock, and K. Bongs, *ibid.* **96**, 180403 (2006).

[27] D. Semmler, K. Byczuk, and W. Hofstetter, Phys. Rev. B **81**, 115111 (2010).

[28] K. Byczuk and M. Ulmke, Eur. Phys. J. B **45**, 449 (2005).

[29] K. Byczuk, M. Ulmke, and D. Vollhardt, Phys. Rev. Lett. **90**, 196403 (2003).

[30] P. Haldar, M. S. Laad, and S. R. Hassan, Phys. Rev. B **95**, 125116 (2017).

[31] D. M. Basko, I. L. Aleiner, and B. L. Altshuler, Ann. Phys. (Amsterdam) **321**, 1126 (2006); M. Serbyn, Z. Papic, and D. A. Abanin, Phys. Rev. Lett. **111**, 127201 (2013); S. Iyer, V. Oganesyan, G. Refael, and D. A. Huse, Phys. Rev. B **87**, 134202 (2013); S. Nag and A. Garg, *ibid.* **96**, 060203(R) (2017).

[32] A. Garg, M. Randeria, and N. Trivedi, Nat. Phys. **4**, 762 (2008).

[33] Y. Anusooya-Pati, Z. G. Soos, and A. Painelli, Phys. Rev. B **63**, 205118 (2001).

[34] Note that there is a difference in convention used for the Δ term in the Hamiltonian in [16] and the current Hamiltonian. The two are related by a factor of 2.

[35] M. Balzer and M. Potthoff, Physica B **359-361**, 768 (2005).

[36] E. H. da Silva Neto *et al.*, Science **343**, 393 (2014); I. M. Vishik *et al.*, Proc. Natl. Acad. Sci. USA **109**, 18332 (2012).

[37] W. A. Atkinson, P. J. Hirschfeld, and A. H. MacDonald, Phys. Rev. Lett. **85**, 3922 (2000); A. Ghosal, M. Randeria, and N. Trivedi, Phys. Rev. B **63**, 020505 (2000); T. S. Nunner, B. M. Andersen, A. Melikyan, and P. J. Hirschfeld, Phys. Rev. Lett. **95**, 177003 (2005).

[38] A. V. Balatsky, I. Vekhter, and J.-X. Zhu, Rev. Mod. Phys. **78**, 373 (2006); D. Chakraborty, R. Sensarma, and A. Ghosal, Phys. Rev. B **95**, 014516 (2017).